

RSC Advances



This is an *Accepted Manuscript*, which has been through the Royal Society of Chemistry peer review process and has been accepted for publication.

Accepted Manuscripts are published online shortly after acceptance, before technical editing, formatting and proof reading. Using this free service, authors can make their results available to the community, in citable form, before we publish the edited article. This *Accepted Manuscript* will be replaced by the edited, formatted and paginated article as soon as this is available.

You can find more information about *Accepted Manuscripts* in the [Information for Authors](#).

Please note that technical editing may introduce minor changes to the text and/or graphics, which may alter content. The journal's standard [Terms & Conditions](#) and the [Ethical guidelines](#) still apply. In no event shall the Royal Society of Chemistry be held responsible for any errors or omissions in this *Accepted Manuscript* or any consequences arising from the use of any information it contains.

Mitoprotective Activity of Oxidized Carbon Nanotubes against Mitochondrial Swelling Induced in Multiple Experimental Conditions and Predictions with New Expected-Value Perturbation Theory

Michael González-Durruthy^{a,b,c,d,*}, Jose Maria Monserrat^{a,b,c,d}, Luciane C. Alberici^e, Zeki Naal^e, Carlos Curti^e and Humberto González-Díaz^{f,g,*}

^a *Institute of Biological Science (ICB), Universidade Federal do Rio Grande (FURG), 90610-000, Porto Alegre, RS, Brazil.*

^b *ICB-FURG Post-graduate Program Physiological Sciences – Comparative Animal Physiology, Brazil, 90610-000, Porto Alegre, RS, Brazil.*

^c *National Institute of Carbon Nanomaterial Science and Technology, Belo Horizonte, MG, Brazil.*

^d *Nanotoxicology Network (MCTI/CNPq), Environmental and Occupational Nanotoxicology, Rio Grande, RS, Brazil.*

^e *Department of Physic-Chemistry, Faculty of Pharmacy of Ribeirão Preto, University of São Paulo (USP), 14040-903 Ribeirão Preto, SP, Brazil.*

^f *Department of Organic Chemistry II, Faculty of Science and Technology, University of the Basque Country UPV/EHU, 48940, Leioa, Bizkaia.*

^g *IKERBASQUE, Basque Foundation for Science, 48011, Bilbao, Bizkaia.*

*** Corresponding authors:**

M. González-Durruthy, FURG (experimental topics), gonzalezdurruthy.furg@gmail.com

H. González-Díaz, UPV/EHU (theoretical topics), humberto.gonzalezdiaz@ehu.es

Abstract: Mitochondrial Permeability Transition Pore (MPTP) is involved in neurodegeneration, hepatotoxicity, cardiac necrosis, nervous and muscular dystrophies. We used different experimental protocols to determine the mitoprotective activity (% P) of different carbon nanotubes (CNT) against mitochondrial swelling in multiple boundary conditions (b_j). The experimental boundary conditions explored included different sub-sets of combinations of the following factors b_0 = three different mitochondrial swelling assays using the MPT-inductor (Ca^{2+} , Fe^{3+} , H_2O_2) combined or not with a second MPT-inductor and swelling control assays using MPT-inhibitor (CsA, RR, EGTA), b_1 = exposure time (0 – 600 s), and b_2 = CNT concentrations (0 – 5 $\mu\text{g/ml}$). Other boundary conditions (b_k) changed were the CNT structural parameters b_3 =CNT type (SW, SW + DW, MW), b_4 =CNT functionalization type (H, OH, COOH). We also changed different of CNT like b_5 =Molecular Weight/Functionalization ratio ($^{\text{min}}\text{W}/^{\text{max}}\text{W}$) or b_6 = Maximal and minimal diameter ($D_{\text{min}}/D_{\text{max}}$) as physic-chemical properties (V_k). Next, we employed chemoinformatics ideas to develop a new Perturbation Theory (PT) model able to predict the %P of CNT in multiple experimental conditions. We investigated different output functions of the absorbance $f(\epsilon_{ij})$ used in PL4/PL5 methods like (ϵ_{ij} , $1/\epsilon_{ij}$, $1/\epsilon_{ij}^2$, or $-\log\epsilon_{ij}$) as alternative outputs of the model. The inputs are in the form an additive functions with linear/non-linear terms. The first term is a function $^0f(\langle\epsilon_{ij}\rangle)$ of the average absorbance $\langle\epsilon_{ij}\rangle$ (expected value) in different assays(b_j). The concentration dependent terms are linear functions of concentration, or hill-shaped curves similar to PL4/PL5 functions (used in dose-response analysis). The CNT structure perturbation terms are linear/non-linear functions of Box-Jenkins operators (ΔV_{kj}). The ΔV_{kj} are moving averages (deviations) of the V_k of the CNT with respect to their expected values $\langle V_{kj}\rangle$. The best model found predicted the values of absorbance (measure of mitoprotective activity vs. mitochondrial swelling) with regression coefficient $R^2 = 0.997$ for > 6000 experimental data points ($q^2 = 0.994$). Last, we used the model to carry out a simulation of the changes on mitoprotective activity for CNT family after one increase of 1-10% of the $^{\text{min}}\text{W}_i$ and $^{\text{max}}\text{D}_i$ of CNT.

Keywords: Carbon Nanotube, Cytotoxicity, Mitochondrial Permeability Transition, Perturbation Theory

INTRODUCTION

Mitochondrial Permeability Transition (MPT) is associated to a higher permeability of the mitochondrial membranes to metabolites and xenobiotics under a threshold value of MW < 1500 Da due to the opening of MPT pore (MPTP)¹⁻⁵. The MPTP is a multi-protein complex that connects the interior and the outer mitochondrial membrane formed by the ADP/ATP carrier or adenine nucleotide translocase (ANT) and the voltage-dependent anion channel (VDAC). Since the discovery of MPTP by Haworth and Hunter in 1979, this biochemical event has been linked to hepatotoxicity, neurodegeneration (*Alzheimer*, *Parkinson*), cardiac ischemia, nervous and muscular dystrophies (amyotrophic lateral sclerosis). In these sense, MPTP has been recognized as a critical factor in the cellular responses under pathological conditions accompanied of osmotic swelling, leading to increases in volume in the mitochondrial matrix, rupture of the outer mitochondrial membrane by opening of membrane pores in mitochondria, dissipation of the membrane potential, increase of reactive oxygen species (ROS) generation and affects the normal ATP levels. This process is triggered by calcium overload, transition metals in concentrations greater than 5 μ M and other pro-oxidant conditions²⁻⁵. Also can trigger conformational changes in inner mitochondrial membrane proteins; oxidation of thiol groups that form the MPTP and release of pro-apoptotic signals (citocrome c, caspase 3, caspase 9), which are closely linked to mitochondria dysfunction mechanisms. Following this idea, the search of new chemical structures able to act as MPTP-inhibitors (mitoprotectors) has become a very important goal. The immunosuppressant drug Cyclosporine A (CsA)⁶ is a one of the best known examples of mitoprotector agent with direct action over this target. Recently research has focused on the effects of structural changes over structure-property relationships of mitoprotectors. For instance, de Farias *et al.*⁶ carried out experimental studies of structure-mitoprotective activity relationships on derivatives of phenothiazine. In other recent study it was evaluated the comparative hepatoprotective effects of tocotrienol analogs by different mechanisms including mitoprotective activity.⁷

In this context, the great potential of applications of carbon nanotubes (CNT) has increased the interest with respect to other carbon biomaterials. The lipophilic character based on its high lipid/water partition coefficient and enough access to the mitochondrial membranes could induce cell death or apoptosis mediated by alteration of bioenergetic mechanisms⁷⁻⁹. Nevertheless is possible to reduce their toxicity through the chemical oxidation as in the case of SW/MWCNT-OH and/or SW/MWCNT-COOH. In this context, Wang *et al.*⁸, demonstrated in structure-property relationships studies that the acid-treated and taurine functionalized multi-walled carbon nanotubes (MWCNT) induced differential pulmonary toxicity in mice. Also, Ye *et al.*¹⁰, examined the mitoprotective effects of multi-wall carbon nanotubes (MWCNT) over osteoclastogenesis in presence of cyclosporine A (CsA) (classical inhibitor of MPTP), rendering MWCNTs as a promising candidate for the treatment of osteoclast-related diseases.

On the other hand¹¹, the combination of different methods is of the major interest for the rational design of nanoscale systems like CNT, iron nanoparticles, micelle nanoparticles, etc. For this reason, Quantitative Structure-Property/Activity Relationships (QSPR/QSAR) methods may play an important role as enabling or complementary tools to experimentation. Tropsha, Leszczynski, Toropov, Puzyn, Roy, Hopfinger, Carbó-Dorca and others¹¹⁻²⁸ have published some of the pioneering works on NQSPR studies of nanoparticles (NQSPR). The main assumption of QSPR/QSAR²⁹⁻³¹ models in general is that similar molecules have similar properties. Consequently, small changes in the structure of the system should correlate linearly with small changes on the values of its properties. Paradoxically, not all similar molecules have similar properties. Very recently, Gonzalez-Díaz *et al.*³², formulated a general-purpose PT-QSPR method combining QSPR/QSAR approach and Perturbation Theory (PT) ideas. PT-QSPR models are very useful for the study of complex molecular systems with simultaneous variation of multiple experimental boundary conditions. In fact, González-Díaz H. *et al.*³²⁻³⁵ have applied PT-QSPR analysis for the study of chemical reactivity, drug metabolism, vaccine epitopes, metabolic networks, and also micelle nanoparticles. In addition, Luan *et al.*³⁶ published the first PT-QSPR model for the cytotoxicity of nanoparticles in multiple experimental conditions. Kleandrova *et al.*^{37, 38} extended the

idea to the PT-QSPR studies of ecotoxicity and cytotoxicity of uncoated and coated nanoparticles under different experimental conditions. Last, Speck-Planche *et al.*³⁹ published the first PT-QSPR model of antibacterial profiles of nanoparticles in multiple experimental conditions.

In this context, it is clear the importance of the development of new mitoprotective drugs studying diverse types of CNT. They may become of the major importance towards both an experimental characterization of CNT in different experimental conditions using a definition of a general model for the prediction of MPT response to different kind of CNT. However, there are no reports of combined experimental and PT-QSPR theoretical studies towards the development of predictive tools for the design of new CNT with mitoprotective activity on MPTP.

In this work, we are going to report the first combined study with experimental-theoretical techniques in this direction. Firstly, we used three different experimental swelling protocols to determine the mitoprotective activity (% P) of different CNT in multiple experimental boundary conditions (b_j). The conditions explored were b_0 = Specifications of the biological assay carried out (MPT-inductor: Ca^{2+} , Fe^{2+} , H_2O_2 ; MPT-inhibitor: CsA, ruthenium red (RR), EGTA, Quercetin (Q) and second MPT-inductor: KCN, Ascorbic acid or VitC), b_1 = exposure time to CNT, b_2 = CNT concentrations, b_3 = CNT type (SW, SW + DW, MW), b_4 = CNT functionalization type (H, OH, COOH). We also changed different of CNT like b_5 = Molecular Weight/Functionalization ratio ($^{\text{min}}\text{W}/^{\text{max}}\text{W}$) or b_6 = maximal and minimal Diameter ($D_{\text{min}}/D_{\text{max}}$) as physic-chemical properties. Next, we developed a new PT-QSPR model of mitoprotective activity. Last, we used the model to predict the values of % P of CNTs as mitoprotective activity in many different experimental conditions or after structural changes.

MATERIALS AND METHODS

Experimental section

Reagents and solutions.

Sucrose, ethyleneglycol-bis (β -aminoethyl)-N,N,N',N'-tetraacetic acid (EGTA), CaCl_2 , KCL, Fe^{2+} -citrate solutions, H_2O_2 , ascorbic acid, cyclosporine A (CsA), ruthenium red (RR), potassium succinate (plus 2 μM rotenone), K_2HPO_4 , piperazine-N₂-ethanesulfonic acid (Hepes-KOH), quercetin, KCN, All other reagents were commercial products of the highest purity grade available. Pristine-carbon nanotubes, hydroxylated carbon nanotubes (CNT-OH) and carboxylated carbon nanotubes (CNT-COOH) were provided by Cheaptubes Company (<http://cheaptubes.com/shortohcnts.htm>).

Carbon nanotubes characterization and stock solutions

Transmission Electron Microscope (TEM, Tecnai G2-12 - SpiritBiotwin FEI - 120 kV) was used to characterize the morphology of pristine and oxidized carbon nanotubes (MWCNT: CNT1; [SWCNT+DWCNT]-OH: CNT2; MWCNT-OH: CNT3, CNT4, CNT5; MWCNT-COOH: CNT6, CNT7, and CNT9; SWCNT-COOH: CNT8) see **Figure 1**. In addition, Raman spectra were measured using a Renishaw Micro-Raman Spectroscopy System (Renishaw plc, Wotton-under-Edge, UK) at room temperature at a laser excitation wavelength of 514 nm (2.33 eV). All reactions were quenched to room temperature before Raman spectra were recorded to identify the characteristic peaks in the position of $1,580\text{ cm}^{-1}$ (G band of graphite) and the peak in the $1,350\text{ cm}^{-1}$ approximately associated to the presence of disorder and/or vacancy defects in the CNT-structure produced by chemical oxidation in the graphite structure (oxidized-CNT with OH and COOH functional groups) as shown in **Figure 2**. The content of metallic impurities in all the samples was less than 5%. The proportions of metal impurities were determined by mass variation as a function of temperature using thermogravimetric analysis. The impurities of MWNT and SWNT with diameter (D) <8nm (CNTs 1, 2, 8 and 9) including their -OH and -COOH derivatives are the same: Co, Fe, Cr, Mg. For MWNT-OH and -COOH 10-20 nm are Co, Ni, Mg and Al (CNTs 4 and 7). For larger diameter MWNT (30-50nm), the metallic impurities and its derivatives are Fe, Ni, Cr, Co, Mg (see Table 1 for details). CNTs were dissolved in dimethyl sulfoxide (DMSO: 900 μL) and ultrapure Milli Q water (10 μL) in individual stock solutions at a concentration of 1 mg/ml. Tip-sonication regime during 5-10 min was used to prevent CNTs agglomeration for MPT-

assays carried out at a range of concentrations of 0.5-5 $\mu\text{g/ml}$. In this sense, the employed sonication time is known to generate a non-agglomerated suspension in a monodisperse state at concentrations below 100 $\mu\text{g/ml}$ according to Bergin et al. (2010). The sonication power was 9.3 W, with an energy input of 16.7 kJ at 25°C using a Ultrasonic/Eco-sonics Q-3.0/40A sonicator. After, samples were stirred for 10-15 min. The resulting diluted suspensions were cooled to room temperature and filtered through a 0.22 μm polycarbonate membrane (Millipore, USA), before exposure to mitochondria suspensions.

Table 1 comes about here

Animal welfare.

Male *Wistar* rats (4-month-old; approx. 200 g) received food and water *ad libitum*. They were kept in plastic cages with wire tops in a light-controlled room (12h light–dark cycle) at 22 ± 2 °C before starting the study in accordance with the Guidelines on the Handling and Training of Laboratory Animals published by the Universities Federation for Animal Welfare (1992).

Isolation of rat-liver mitochondria.

We used standard differential centrifugation to isolate the Mitochondria⁴⁰. Male *Wistar* rats weighing approximately 200 g were euthanized by decapitation; livers (10–15 g) were immediately removed, sliced in medium (50 ml) consisting of 250 mM sucrose, 1 mM ethyleneglycol-bis (β -aminoethyl)-N,N,N',N'-tetraacetic acid (EGTA) and 10 mM HEPES-KOH, pH 7.2, and homogenized three times for 15 s at 1 min intervals using a Potter-Elvehjem homogenizer. Homogenates were centrifuged (580 g, 5 min) and the resulting supernatant further centrifuged (10,300 x g, 10 min). Pellets were then suspended in medium (10 ml) consisting of 250 mM sucrose, 0.3 mM EGTA and 10 mM HEPES-KOH, pH 7.2, and centrifuged (3,400 x g, 15 min). The final mitochondrial pellet was suspended in medium (1 ml) consisting of 250 mM sucrose and 10 mM HEPES-KOH, pH 7.2, and used within 3 h. Mitochondrial protein contents were determined by the Biuret reaction.⁴¹

Standard incubation procedure.

Mitochondria isolated were energized with 5 mM potassium succinate (plus 2.5 μM rotenone) in a standard incubation medium consisting of 125 mM sucrose, 65 mM KCl, 2 mM inorganic phosphate (K_2HPO_4) and 10 mM HEPES-KOH pH 7.4 at 30 °C⁴¹.

Determinations of MPT induction in different conditions.

MPT was measured through monitoring the decrease in apparent absorbance of the mitochondrial suspension measured at 540 nm in a Hitachi U-3000 spectrophotometer equipped with magnetic stirring and temperature control (28 °C).⁴² Mitochondria were incubated in the standard incubation medium at 1 mg of mitochondrial protein/ml. Before the spectrophotometric MPT-measurements the blanks with CNTs were run to compare with mitochondria exposed to CNT and interferences of carbon nanotubes were not observed at 400-550 nm. MPT was induced by three different experimental conditions: **1)** Swelling assay induced by Ca^{2+} 20 μM , for this instance, we designed three protocols using different MPT-inhibitors controls as CsA 1 μM a known classic MPT-inhibitor of mitochondrial swelling induced by calcium overload; Ruthenium red (RR), 1 μM an specific blocker of mitochondrial calcium uniporter that interferes with Ca^{2+} influx from cytoplasm to mitochondrial matrix and EGTA 100 μM as chelating agent. The combinations tested were: [Ca^{2+} 20 μM]; [Ca^{2+} 20 μM +CsA 1 μM]; [Ca^{2+} 20 μM +RR 1 μM]; [Ca^{2+} 20 μM + EGTA 100 μM] to represent MPT-inhibition (100%) and [Ca^{2+} 20 μM + CNTs]; **2)** For swelling assay induced by Fe^{2+} 20 μM were used as MPT-inhibitors control (EGTA 100 μM) and additional control as second MPT-inductors to recreate synergistic action on MPT. Followed this idea it was used (KCN 1 μM : indirect MPT-inductor by inhibition of cytochrome c oxidase associated to ROS-formation; Ascorbic acid or Vit C 100 μM : a strong reducing agent that induce similarly MPT based in ROS-generation). For this instance, the combinations evaluated were: [Fe^{2+} 20 μM], [Fe^{2+} 20 μM +EGTA 100 μM](100% of MPT-inhibition), [Fe^{2+} 20 μM +CNTs]. For evaluate the maximum value of MPT-induction induced by iron we performed the following combinations in order to mitotoxic potential: [Fe^{2+} 20 μM +VitC 1 μM +CNTs,5 $\mu\text{g/ml}$] > [Fe^{2+} 20 μM +KCN 1 μM +CNTs,5 $\mu\text{g/ml}$] > [Fe^{2+} 20 μM +CNTs]. Please note that this conditions proposed are propitious to induce mitochondrial

permeability transition based in Fenton-Haber-Weiss reaction. **3)** Swelling assay induced by H₂O₂ 300 μM in this test was used Fe²⁺ 20μM as second MPT-inductors to recreate synergistic action on MPT based in pro-oxidant conditions(Fenton-Haber-Weiss reaction) and Quercetin 50 μM (Q: MPT-inhibitor, known antioxidant, employed as control based in ROS-inhibition that prevent the MPTP-thiols group oxidation associated to MPT-induction in pro-oxidant conditions). The combinations tested were [H₂O₂ 300μM], [H₂O₂ 300μM+Quercetin 50 μM] (100% of MPT-inhibition in pro-oxidant conditions), [H₂O₂ 300μM+CsA 1μM], [H₂O₂ 300μM+CNTs], [H₂O₂ 300μM+ Fe²⁺ 20μM+ CNTs, 5 μg/ml] (100% of MPT-induction in pro-oxidant conditions). These three mitochondrial swelling protocols: **1.** Ca²⁺ 20μM, **2.** Fe²⁺ 20μM, and **3.**H₂O₂ 300μM; were performed in the presence of CNT in different concentrations (0-5 μg/ml) to investigate in parallel the mechanisms and factors directly or indirectly involved in MPTP-inhibition. All the swelling experiments where the second MPT-inductor is present were performed with the highest concentration (5 μg/ml) to challenge the mitoprotective potential of CNT^{41, 43-48}. In addition, we considered other factors as metal impurities. In this context, the maximum expected concentration of metal impurities should be 0.25 μg/ml (5% of the highest concentration in the CNTs samples) which possess no risk of MPT induction in this low levels¹⁻⁵. In **Figure 3**, we illustrate the workflow of this experimental section.

Figure 3 comes about here

Microscopy analysis of mitochondrial swelling induction associated to membrane potential

The suspension of isolated rat-liver mitochondria were pre-incubated with a specific mitochondrial dye (JC-1) in 0.2 mg/ml for 15 min according Reers *et al.*⁴⁹. Images were analyzed using a fluorescent microscope (Olympus IX81, Markham, Ontario, Canada) equipped with a DP72 digital camera to study the effects of different mitochondrial swelling assays associated with the loss mitochondrial membrane potential (red to green fluorescent) after incubation with a MPT-inductor (Ca²⁺, Fe²⁺, or H₂O₂) and in the presence or the absence of a MPT-inhibitor (CsA, RR, EGTA or one kind of CNT).

Theoretical section

Theoretical details of the PT-NQSPR models.

Very recently, Gonzalez-Díaz *et al.*³³ formulated a general-purpose Perturbation Theory (PT) model for Chemoinformatics problems with multiple-boundary experimental conditions. In this work, we are going to re-formulate this theory in order to develop a new type of PT-QSPR models for Nanomaterials (PT-NQSPR models). In **Figure 4**, we illustrate the workflow for this theoretical part. Specifically, the new PT-NQSPR models developed here are expected values to predict the effect of different CNT structures in three different MPT induction assays under multiple experimental boundary conditions. The PT-NQSPR model proposed here is an additive equation with linear/non-linear terms expressed in the following form:

$$f(\varepsilon_{ij})_{\text{new}} = e_0 + a_0 \cdot f(\varepsilon_{ij})_{\text{ref}} + \sum_{k=1}^{k_{\text{max}}} a_k \cdot f(\Delta V_{kj}) \quad (1)$$

$$f(\varepsilon_{ij})_{\text{new}} = e_0 + a_0 \cdot f(\varepsilon_{ij})_{\text{ref}} + \sum_{k=1}^{k_{\text{max}}} a_k \cdot ({}^k V_i - \langle {}^k V_{ij} \rangle) \quad (2)$$

We used Multivariate Linear Regression (MLR) and Non-Linear Regression (NLR) algorithms implemented in the software STATISTICA⁵⁰ to determine the values of the coefficients (a_k) and other parameters of the model. In our PT-NQSPR model, the output $f(\varepsilon_{ij})_{\text{new}}$ is a function of the expected absorbance. In the simplest case we use the identity function and $f(\varepsilon_{ij})_{\text{new}} = \varepsilon_{ij}$ is equal to the predicted absorbance value under the new sub-set of experimental boundary conditions of reference. Other transformation functions applied to ε_{ij} were: $f(\varepsilon_{ij}) = 1/\varepsilon_{ij}$, $(1/\varepsilon_{ij})^2$, or $-\log(\varepsilon_{ij})$, see **Table 2**.

In addition, we are going to consider different sub-sets of input experimental boundary conditions of reference ${}^{\text{ref}}b_j \equiv (b_0, b_1, b_2, b_3 \dots b_6)$. In the equation we introduced one specific input term to quantify

each one of these conditions. The elements of the vectors $\mathbf{v}_i = [{}^0f(\varepsilon_{ij})_{\text{ref}}, {}^1f(\Delta V_{1,j}), \dots, {}^2f(\Delta V_{2,j}), \dots, {}^{k_{\text{max}}}f(\Delta V_{k_{\text{max},j})]$ are the inputs of this model.

Figure 4 comes about here

This first term of this PT-NQSPR model is the function ${}^0f(\varepsilon_{ij})_{\text{ref}} = \langle \varepsilon_{ij} \rangle_{\text{new}}$. This function is the average of absorbance value for all CNTs measured under the experimental conditions of the output. It means that we could interpret ${}^0f(\varepsilon_{ij})_{\text{new}}$ as the new expected value of absorbance for CNTs measured under the same sub-set of experimental conditions (for a normal distribution).

Following this idea were incorporated the ΔV_{kj} parameters as the second class of terms, which are functions of the Box-Jenkins operators (moving average) used here as perturbation terms ${}^k f(\Delta V_{k,j})$. The functions ${}^k f$ represent transformations ${}^k f(\Delta V_{k,j})$ of the moving averages $\Delta V_{k,j}$ of the original input variables ${}^k V_i$ for i-th type of CNT in j-th MPT-assay of one specify boundary condition b_{kj} .

The value $\langle V_{kj} \rangle$ is interpreted as the average of the k-th physicochemical properties (${}^k V_{ij}$), see the equation 3:

$$V_{kj} = \frac{1}{n_j} \left(\sum_{i \in j} {}^k V_{ij} \right) \quad (3)$$

This (${}^k V_{ij}$) of CNT was used to quantify the effect over the output ${}^0f(\varepsilon_{ij})_{\text{new}}$ of perturbations on different experimental boundary conditions (b_j). The following set of conditions are related to the CNT-structure, b_3 =CNT type (SW, SW + DW, MW), b_4 =CNT functionalization type (H, OH, COOH), b_5 = CNT chemical function (OH, COOH, or none) in term of Molecular Weight/Functionalization ratio and b_6 = maximal and minimal diameter ($D_{\text{min}}/D_{\text{max}}$) and for b_0 = multiple experimental boundary conditions. That include the average of the values with the same conditions as mitochondrial swelling assays using the MPT-inductor (Ca^{2+} , Fe^{3+} , H_2O_2 , or none) or toxic control $\text{TC}_1(+)$, second MPT-inductor (KCN, VitC, or none) or second toxic control $\text{TC}_2(+)$, MPT-inhibitors or inhibitor control $\text{IC}_1(-)$ (CsA or none) and non-classical MPT-inhibitor control (RR, EGTA, Quercetin, or none). Last, included other conditions related to the assay like, Solvent (DMSO, or none), Replicate sample (Yes, No).

For instance, for exposure time the condition b_1 = exposure time (t_{ij}) of samples corresponding to the i-th CNT used in b_j -th MPT-assay. Some of the functions used to transform these variables where: ${}^1f(\Delta t_{ij}) = 1/(\Delta t_{ij})$, $\exp(-\Delta t_{ij})$, and the other b_2 = concentration (c_{ij}) of i-th CNT in the j-th assay is ${}^2f(\Delta c_{ij}) = 1/\Delta c_{ij}$ or $1/(1+\Delta c_{ij})$ for CNT concentration. In addition other functions as ${}^3f(\Delta W_{ij})$ to Molecular Weight/Functionalization ratio (b_5), ${}^4f(\Delta D_{ij})$ for maximal and minimal diameter (b_6) (see **Table 2**).

Table 2 comes about here

RESULTS AND DISCUSSION

Experimental Measure of CNT-MPT modulation in different conditions.

The important role of mitochondria to regulate intracellular calcium levels has been associated with several chronic diseases as neurodegenerative diseases, cardiovascular and cancer, which currently have high levels of morbidity and mortality⁵¹. In this study, we performed three experimental protocols to evaluate the effect of CNT in mitochondrial permeability transition (swelling) induced by different mechanisms, basing each experimental protocol on the causes and factors that trigger this process, as Ca^{2+} overload in the mitochondrial matrix and loss of redox balance under conditions of iron overload and high peroxide production. Under these conditions, the physic-chemicals properties of CNT family were evaluated and linked to their capacity for the inhibition of MPT^{52, 53}. For this instances the CNT-interferences in spectrophotometric MPT-measurements it were not detected based on the non-existence of the classic UV-visible absorption peaks of mitochondrial redox hemoprotein (408 to 550 nm) as oxidized cytochrome c (Fe^{3+}) at 408 nm and 530 nm and three peaks of reduced cytochrome c (Fe^{2+}) at 415 nm, 520 nm, and 550 nm when we monitored the decrease in absorbance of the mitochondrial suspension measured at 540 nm used to evaluate the mitochondria swelling in the presence of carbon nanotubes as mentioned in Materials and Methods section.⁵²

At first, we evaluated the effect of CNT family on MPT induced by Ca^{2+} 20 μM , which has been described in many pathological conditions as cancer, neurodegenerative diseases and ischemia-reperfusion processes¹⁻³.

In this sense, the selective MPT-modulation with CNT could lead to alternatives for the treatment of cancer and its inhibition may prevent cell and tissue damage associated with a number of diseases. The isolated mitochondria exposed to high calcium concentrations are susceptible to the opening of mitochondrial permeability transition pore, the larger implications of this phenomenon are the diffusion of solutes of up to 1500 Dalton, through the inner mitochondrial membrane, depletion of ATP levels and dissipation of mitochondrial membrane potential as illustrated in **Figure 5**. These effects are accompanied by mitochondrial swelling caused by the osmotic difference between the mitochondrial matrix and the extra-mitochondrial medium, followed by outer membrane rupture and release of proapoptotic signals (caspases 3 and 9) from the inter-membrane space^{3,4}.

Figure 5 comes about here

Firstly the calcium dependence on MPT was verified by different mechanism, performing teste in the presence of Ca^{2+} (20 μM) with CsA that inhibits the binding of Ca^{2+} to cyclophilin D, in this condition calcium overload produce conformational changes that induce MPT⁵⁴ (assay P₁). Also, other non-specific MPT-inhibitors controls were evaluated as EGTA, a calcium chelating agent (assay P₂) and ruthenium red (RR), which interfere in the Ca^{2+} uptake by the mitochondrial uniporter⁵⁵ (assay P₃). All these tests were conducted as experimental controls to express the maximum of mitoprotective activity (% P) by different mechanisms.

Swelling assays was performed to study the MPT-effects of CNT family induced by Ca^{2+} 20 μM to find similarities or differences in the pattern of inhibition between CNT family and classic and non-classical MPT-inhibitor controls as showed in **Table 3**. The results showed low capacity of CNT family to inhibit the MPT induced by Ca^{2+} 20 μM in most cases, when compared with CsA, the main specific inhibitor of MPT pore induced by calcium overload and also using non-specific MPT-inhibitors controls (EGTA 100 μM , RR 1 μM) used as negative control or MPT-inhibitors⁵⁵.

Several aspects must be considered to explain the low and variable MPT inhibition induced by CNT family against mitochondrial Ca^{2+} overload. First, CNT should cross the outer mitochondrial membrane, mitochondrial inter-membrane space, and matrix, process that should be facilitated in virtue of its high lipid partition coefficient/water⁵⁶. However the modest mitoprotective effects (% P) found may be related with certain structural characteristics of CNT family. In this sense, higher % P consistent with a decreased of mitochondrial swelling induced by Ca^{2+} was observed for functionalized CNT, following the order CNT-COOH (MWCNT-9, MWCNT-7, SWCNT8, MWCNT-6) > CNT-OH (SWCNT-2, MWCNT-3, MWCNT-5, MWCNT-4) > pristine MWCNT (MWCNT-1). According to the mitoprotective values (% P), CNT-9 is the more mitoprotector and CNT-1 is mitotoxic. We suggest a mechanism based in Ca^{2+} adsorption by carboxyl groups (COO⁻) of CNT-COOH, which should reduce the free concentration of this divalent ion in the mitochondrial matrix. Chemical adsorption capacity of oxidized CNT has been demonstrated in other nanoQSAR studies using aromatic organic and inorganic MPT inductors.⁵⁷ Also for carboxylated-CNT, specifically CNT-7, CNT-8, and CNT-9 it was observed a significant increase of % P at higher concentrations (3.0 and 5.0 $\mu\text{g/ml}$). The lower %P of hydroxylated-CNT compared with their similar carboxylated-CNT could be related with a lower Ca^{2+} adsorption capacity, although higher when compared with similar pristine-CNT, that presented mitotoxic effect.⁵⁷

In this case, the absence of COOH functionalization (MWCNT) could generate mitotoxic effects based in this mechanism and, under this context, the toxicity of carbon nanomaterials should be reduced through the chemical oxidation as in the case of CNT-OH and CNT-COOH according to Zhenbao *et al.*⁵⁸. Other possible inhibitory mechanisms could be the interaction of carboxyl groups of carboxylated-CNT with positive NH_2 groups of VDAC and ANT to prevent conformational changes necessary for MPTP components assembly and apoptosis⁵⁹⁻⁶¹. A significant number of studies have demonstrated that

MPT-modulation is mediated by conformational changes of VDAC and ANT located on the outer and inner mitochondrial membrane respectively⁶¹⁻⁶³.

Next, experiments were performed to study the MPT-effects induced by iron overload for CNT family. Iron overloading has been proposed to cause dissipation of membrane potential and increase of calcium efflux in mitochondria dynamics that are often associated with loss of redox balance, involving oxidation of MPT pore-sulfhydryl groups⁶⁴⁻⁶⁶. For this instance were conducted swelling assays in the presence of Fe^{2+} 20 μM . Also it were considered other more aggressive mitotoxic or condition of synergism to enhance the MPT-effects of iron overload combining separately with KCN 1 μM , an inhibitor of mitochondrial complex IV (cytochrome c oxidase) and consequently of the electrons transport chain (assay P₂). Also with ascorbic acid 300 μM , a strong reducing agent that favors the reduction of Fe^{3+} to Fe^{2+} and thus inducing pro-oxidant states (assay P₃)^{53,67}. Both non-classical MPT inductors and second inductor were used as positive controls to challenge the mitoprotective potential of CNT family to reverse mitochondrial swelling induced by Fe^{2+} 20 μM ⁶⁸. Under this protocol, EGTA 100 μM was used as negative control or MPT-inhibitors as show in **Table 4**.

Table 4 comes about here

Mitoprotective activity (%P) was higher for carboxylated-CNT and hydroxylated-CNT in comparison with the lowest % P of pristine-CNT, more mitotoxic, results that fits with a previous study that reported increased cytotoxicity to pristine CNT in relation to the functionalized-CNT.⁶⁹ It is important to note that the % P of CNT family was considerably higher to Fe^{2+} swelling than to Ca^{2+} swelling tests. But in both cases the response pattern was similar, according to the functionalization type: CNT-COOH (MWCNT-9, MWCNT-7, SWCNT8, MWCNT-6) > CNT-OH (SWCNT-2, MWCNT-3, MWCNT-5, MWCNT-4) > pristine-CNT (MWCNT-1). A direct chelation of mitochondrial iron has been suggested as an attractive therapeutic strategy for several clinical disorders involving iron imbalance⁵³. In present study, the inhibition of MPT could involve the interaction of the COOH and OH groups of oxidized-CNT with the reduced state (Fe^{2+}) of heme group in the mitochondrial complexes I and III, known to be mitochondrial ROS producers. This interaction should form a coordination complex between the oxidized-CNT and the metallic center, helping to reduce the levels of ferrous ions (Fe^{2+}), preventing Fenton-Haber-Weiss reaction that leads to the generation of hydroxyl radical⁵³. Following this idea, we suggest a possible mechanism based on iron coordination by COOH and OH groups of the CNT combined with chemical adsorption mechanisms onto oxidized-MWCNT to reduce the excess in the Fe^{2+} free concentrations, thus preventing mitochondrial swelling in pro-oxidant conditions^{53,58}. The P% for the MPT-assay using the [Fe^{2+} 20 μM +KCN 1 μM +CNTs, 5 $\mu\text{g}/\text{ml}$] (P₂) showed a similar behavior to MPT-assay using [Fe^{2+} 20 μM +CNTs,5 $\mu\text{g}/\text{ml}$] (P₁) in the order carboxylated-CNT > hidroxylyated-CNT > pristine-CNT for mitoprotetive activity (% P). The evidences suggest therapeutic potential of oxidized nanotubes to reverse the swelling induced by Fe^{2+} overload despite the participation of uncoupling mitochondrial mechanisms as KCN 1 μM , which acts synergistically favoring the opening of MPT-pore. However only carboxylated-CNT (5) and hidroxylyated-CNT (2, 3, 6) were able to reverse the pro-oxidant effects generated by iron overload combined with ascorbic acid 300 μM , a strong reducing agent. Also according to the walls number, it was observed higher values of mitoprotection in the order MW-motifs > SW+DW-motif > SW-motifs, these evidences are coherent with studies performed using K562 and HeLa cells cultured in the presence of SWCNT, SWNTs-OH, MWCNT-COOH at concentrations ranging from 1 to 100 $\mu\text{g}/\text{ml}$ based in inhibition of telomerase activity.⁵⁹

Finally, assessments were performed to analyze the potential of CNT family to reverse the MPT induced in pro-oxidant conditions of high mitochondrial H_2O_2 levels as shown in **Table 5**. It was performed mitochondrial swelling assays in the presence of H_2O_2 300 μM and using a known antioxidant, Quercetin 50 μM as negative MPT-control as [H_2O_2 300 μM +Quercetin 50 μM] (assay P₁).⁷⁰ The same protocol was run taking CsA 1 μM as [H_2O_2 300 μM +CsA 1 μM] a negative additional MPT-control (assay P₂). Also it was performed a mitochondrial swelling assay induced by H_2O_2 300 μM using Fe^{2+} 20 μM to produce MPT-synergism conditions, for this instance the combination [H_2O_2

300 μ M+ Fe²⁺ 20 μ M + CNTs, 5 μ g/ml] (assay P₃) was employed, to intensify the pro-oxidant conditions. In this case it was also used quercetin 50 μ M as negative MPT-control of references to find similarities or significant differences in the MPT-modulation based in pro-oxidant induced by H₂O₂ 300 μ M of CNT family.

Table 5 comes about here

% values mitoprotection of CNT family were remarkably high in the swelling assays P₁ and P₂ except for pristine-CNT. The result showed % P very similar between CNT-COOH and CNT-OH in the conditions listed above to mitochondrial swelling assays induced by Ca²⁺ and Fe²⁺ at 20 μ M. This suggests that OH and COOH functionalization are important to reverse the mitochondrial swelling associated to pro-oxidant conditions⁷¹. The high %P values of functionalized-CNT exhibited a similar pattern of inhibition, when compared with the two controls used quercetin 50 μ M (non-specific MPT-inhibitors) and CsA 1 μ M (specific MPT-inhibitors), pointing that the inhibition of functionalized-CNT could be associated with the ability to attenuate the loss of redox balance induced by H₂O₂ overload^{51, 53}.

The mitochondria has an efficient antioxidant defense system, including superoxide dismutase, glutathione peroxidase, glutathione reductase, reduced glutathione, NAD(P)⁺ and other cofactors. In physiological conditions the mitochondrial superoxide dismutase transforms the superoxide radical (O₂[•]) to the less reactive H₂O₂, which is reduced to H₂O by the action of GSH and glutathione peroxidase⁵¹.

However, several mito-pathological conditions as peroxide overload (300 μ M) reduced the antioxidant defenses and increases oxidative stress by H₂O₂ accumulation, in our study. The presence of Fe²⁺ induces formation of hydroxyl radical ([•]OH) through Fenton-Haber-Weiss reaction involved in the oxidation of thiol groups constituents of MPTP. In the case of assay P₃, only the highest concentration, 5 μ g/ml was able to reverse the mitochondrial swelling induced by pro-oxidant condition⁵¹ similar to Quercetin 50 μ M⁷⁰⁻⁷². The obtained results should contribute for the rational design of novels carbon nanomaterial and point the way to new areas of research as Mitochondrial Nanomedicine^{73,74}, based in the effects of carboxylated and hydroxylate carbon nanotubes on mitochondrial permeability transition.

PT-NQSPR model in multiple boundary conditions.

In classic response-concentration models, we can use alternative forms of the hill-shaped curve to seek a dose-response equation in order to calculate IC₅₀ values⁵⁰. For instance, the software MasterPlex (<http://psg.hitachi-solutions.com/masterplex>) allows to choose different algorithms such as: 4 parameters logistic (4PL), 5 parameters logistic (5PL), quadratic log-logit, log-log or linear model. The reader can see examples of the use of this software and these algorithms by Tenorio *et al.* in previous works⁵¹⁻⁵⁵. However, the 4PL and 5PL forms have some drawbacks. Some authors have reported studies towards the search of alternatives models to these curves. For instance, Liao *et al.* (2009) reported a re-parameterization of 5PL dose-response curve⁷⁵. In any case, almost all of these alternatives fail when we need to account for multiple experimental boundary conditions (b_j). It means that the model fails when we want to predict the response ε_i for the ith compound not only for different concentrations of the compound (c_i) in a single assay. This points to the need of a model able to predict multiple responses ε_{ij} for the same ith compound when we change multiple boundary conditions like b₀ = multiple experimental conditions of j-th MPT-assays, b₂ = different values of concentration c_{ij} for the compound on the different j-th MPT-assays, different exposure time (0 – 600 s) to the compound b₁ = t_{ij}. We can talk here also of different structural or physicochemical properties of the compound under study. For instance, in the case of CNT we consider the CNT type, b₃ = Single-Walled (SW), Multiple-Walled (MW), or mixtures of SW+DW. In these cases, 4PL/5PL and similar models are unable to fit all the data at the same time and we need to seek a different equation for each sub-set of changing boundary conditions b_{kj}. In this work, we propose by the first time a PT-NQSPR model able to account for changes in multiple experimental boundary conditions (b_j). The general formula of this models the following:

$${}^1f(\varepsilon_{ij})_{\text{new}} = e_0 + a_0 \cdot \langle \varepsilon_{ij} \rangle_{\text{new}} + a_1 \cdot {}^1f(\Delta t_{ij}) + a_2 \cdot {}^2f(\Delta c_{ij}) + a_3 \cdot {}^3f(\Delta W_{ij}) + a_4 \cdot {}^4f(\Delta D_{ij}) \quad (5)$$

$${}^1f(\varepsilon_{ij})_{\text{new}} = e_0 + a_0 \cdot \langle \varepsilon_{ij} \rangle_{\text{new}} + a_1 \cdot {}^1f(t_i - \langle t_{ij} \rangle) + a_2 \cdot {}^2f(c_i - \langle c_{ij} \rangle) + a_3 \cdot {}^3f(W_i - \langle W_{ij} \rangle) + a_4 \cdot {}^4f(D_i - \langle D_{ij} \rangle) \quad (4)$$

We can compare the equation above with the compact notation presented in the Materials and Methods section. In this PT-NQSPR model we can also use (like in 4PL/5PL models) optional weighting schemes for the response variable (output function): ${}^1f(\varepsilon_{ij}) = \varepsilon_{ij}$, $1/\varepsilon_{ij}$, $(1/\varepsilon_{ij})^2$, or $-\log(\varepsilon_{ij})$. We can incorporate different functions ${}^0f = \langle \varepsilon_{ij} \rangle$ of the expected value of ε_{ij} for a sub-set of conditions (e.g., different MPT-assays). We can also use different functions for the input variable; such as: ${}^1f = \Delta t_{ij}$, $1/\Delta t_{ij}$ or $\exp(-\Delta t_{ij})$ for exposure time, or ${}^2f = \Delta c_i$, $1/\Delta c_i$ or $1/(\Delta c_i)^2$ for CNT concentration. A particular case is when the concentration function takes the classic form of PL4/PL5 models⁷⁶. This equation is represented through a sigmoid curve. The formula below illustrates two examples of alternative models following the equation 6:

$${}^2f(\Delta c_{ij}) = A + D \cdot \left\{ I + \left[\left(\frac{\Delta c_{ij}}{C} \right)^B \right] \right\}^{-E} = {}^2f(\varepsilon_{ij})_{\min} + {}^2f(\varepsilon_{ij})_{\max} \cdot \left\{ I + \left[\left(\frac{\Delta c_{ij}}{C} \right)^B \right] \right\}^{-E} \quad (6)$$

The parameters of 4PL/5PL models are: A, B, C, D, and E. A is the value for the minimum asymptote. B is the hill slope. C is the concentration at the inflection point. D is the ε_{ij} for the maximum asymptote. The last parameter E, is present only on 5PL model ($E = 1$ in 4PL model), is the asymmetry factor ($E \neq 1$ for a non-symmetric curve)⁷⁶.

PT-NQSTR model for Mitoprotective activity of CNTs. The ε_i values are obtained after exposure of the mitochondrial suspension to one volume of 100 μL of CNT at different c_i values. We used physicochemical parameters of CNTs (V_{kj}) and the values of the Box-Jenkins Operators (ΔV_{kj}) of these parameters as inputs of the model in statistical analysis. The best PT-QSPR model found using MLR algorithm and linear operators (functions) of $\Delta V_{k,j}$ was the following:

$$\begin{aligned} {}^{\text{new}}\varepsilon_{ij} &= 1.001191 \cdot \varepsilon_{ij \text{ new}} - 0.000066 \cdot \Delta t_{ij}(\text{s}) + 0.002344 \cdot \Delta c_{ij}(\mu\text{g/ml}) \quad (7) \\ &- 0.001191 \cdot \Delta W_{ij}(\)_{\max} - 0.000688 \cdot \Delta D_{ij}(\text{nm})_{\min} + 0.000086 \\ N &= 6045 \quad R^2 = 0.75 \quad F = 2482.1 \quad p < 0.005 \end{aligned}$$

As we mentioned above, in the simplest case the output function ${}^1f(\varepsilon_{ij})_{\text{new}} = {}^{\text{new}}\varepsilon_{ij}$ is the value of absorbance predicted by the linear model under the set of boundary conditions of test of reference. $N =$ number of cases used to train the model, R^2 the determination coefficient, and F the Fisher ratio with the corresponding p -value are the statistical elements used to describe the statistical significance and goodness-of-fit of the model. We can expand the input terms and substitute each symbol $V_k(b_j)$ by the classic symbol of the respective property in order to understand better this equation. The model predicts values of absorbance ${}^{\text{new}}\varepsilon_{ij}$ when assaying the i^{th} CNT in a new experimental situation (j^{th} set of conditions) given the expected values of reference calculated from the data set. The correlation between the inputs and the answer is statistically significant according to p -error values ($p < 0.005$). The values R^2 are high (75% of variance explained) but, unfortunately, we can observe an important dispersion of data points from the straight line in **Figure 6 (A)**.

Figure 6 comes about here

We carry out some transformations of output ${}^0f(\varepsilon_{ij})$ and/or input functions in order to increase the R^2 and decrease the dispersion. The transformation of the output function ε_{ij} were: ${}^1f(\varepsilon_{ij}) = 1/\varepsilon_{ij}$, $(1/\varepsilon_{ij})^2$, or $-\log(\varepsilon_{ij})$. Some of the transformations of the input functions ${}^k f(\Delta V_{kj})$ were ${}^1f(\Delta t_{ij}) = 1/(\Delta t_{ij})$, $\exp(-\Delta t_{ij})$ and ${}^2f(\Delta c_{ij}) = 1/\Delta c_{ij}$ or $1/(1+\Delta c_{ij})$, between others (see details on Materials and Method section). In **Table 6** we depict the results obtained after some of these transformations. The transformation of the output function into a logarithmic function have lead to an outstanding increase in the determination coefficient from $R^2 = 0.75$ to $R^2 = 0.994$ (**Model 2**) with respect to the linear model (**Model 1**). This result also supposed a notably reduction on the dispersion of data, see **Figure 6 (B)**.

We can note that other transformations of inputs variables like Δc_{ij} and Δt_{ij} do not improved the results of the regression (**Models 3 and 4**). In particular, the transformation of the Δc_{ij} function into hill-shaped curves of common use in dose-effect studies was not effective (**Model 5**). In addition, the transformation of both output and input functions at the same time increased the correlation but as a result we obtained a more complex model with loss of statistical significance ($p > 0.05$) for some input variables (**Model 6**). In closing, the best PT-NQSPR model found here was the one using the negative logarithmic transformation for the output. The model have also a very high validation regression coefficient $q^2 = 0.994$, obtained in Leave-One-Out (LOO) cross-validation. The model equation is the following:

$$\begin{aligned} \text{}^{new}\log(\varepsilon_{ij}) &= 1.33764 \varepsilon_{ij \text{ new}} - 0.000001 \cdot \Delta t_{ij}(\text{s}) + 0.00381 \cdot \Delta c_{ij}(\mu\text{g/ml}) \quad (8) \\ &+ 0.000422 \cdot \Delta W_{ij}(\%)_{\text{max}} + 0.000442 \cdot \Delta D_{ij}(\text{nm})_{\text{min}} - 0.927714 \\ N &= 6045 \quad R^2 = 0.994 \quad F = 203384.0 \quad p < 0.005 \quad q^2 = 0.994 \end{aligned}$$

We presented the previous equation in a compacted form for the sake of simplicity. However, we want to give also the expanded form of the equation to make easier the understanding of the method. In the following equation, we expanded each moving average term. It can be noted that each term quantifies the deviation (perturbation) of the original variable (t_{ij} , c_{ij} , W_{ij} , or D_{ij}) from its average value ($\langle t_{ij} \rangle$, $\langle c_{ij} \rangle$, $\langle W_{ij} \rangle$, or $\langle D_{ij} \rangle$). In this sense, each moving average term account for the deviation of the original variable from its expected value (the average value).³³⁻³⁹

$$\begin{aligned} \text{}^{new}\log(\varepsilon_{ij}) &= 1.33764 \cdot \varepsilon_{ij \text{ new}} - 0.000001 \cdot (t_{ij} - \langle t_{ij} \rangle) + 0.00381 \cdot (c_{ij} - \langle c_{ij} \rangle) \quad (9) \\ &+ 0.000422 \cdot (W_{ij} - \langle W_{ij} \rangle)_{\text{max}} + 0.000442 \cdot (D_{ij} - \langle D_{ij} \rangle)_{\text{min}} - 0.927714 \\ N &= 6045 \quad R^2 = 0.994 \quad F = 203384.0 \quad p < 0.005 \quad q^2 = 0.994 \end{aligned}$$

Table 6 comes about here

Prediction of mitoprotective activity of CNT in other conditions. We can use the previous PT-QSPR model to carry out a computational simulation of mitoprotection by CNT in other conditions (not measured experimentally). In so doing, we need to substitute three different types of values in the equation. The first is the expected value of absorbance $\langle \varepsilon_{ij} \rangle_{\text{ref}}$ for a given sub-set of experimental conditions or assay (b_{ij}). We also need to substitute the average values of the physic-chemical properties of the CNTs $\langle V_k \rangle$ in these sub-sets of different experimental conditions $\langle V_{kj} \rangle$, see **Table 7** (right).

Table 7 comes about here

Last, we need to substitute the values V_k for CNTs with different physic-chemical properties not assayed before. In this way, we can obtain new values of absorbance predicted for new CNT with changes in the original physic-chemical properties. Thus we can predict the values of mitoprotection P (%) using the values of ε_{ij} predicted and the values observed with MPT-inductor or toxic control (TC+) and solvent blank. The equation used was the following $P(\%)_{\text{pred}} = 100 \cdot [\varepsilon_{ij}(\text{CNT} + \text{TC} + \text{S})_{\text{pred}} - \varepsilon_{ij}(\text{TC} + \text{S})_{\text{obs}}] / [\varepsilon_{ij}(\text{IC} + \text{TC} + \text{S})_{\text{obs}} - \varepsilon_{ij}(\text{TC} + \text{S})_{\text{obs}}]$ ^{78,79}. In **Table 8**, we show the prediction of $P(\%)_{\text{pred}}$ if we increase at the the same time the maximal molecular weight to functionalization ratio $^{\text{max}}W$ and the minimal $^{\text{min}}D$ of the CNT in $x(\%)$ at $t(\text{s}) = 600$ seg and $c_{ij} = 2.5 \mu\text{g/ml}$. The effect of dose or concentration (1-5 $\mu\text{g/ml}$) influenced poorly the model and, for this reason, an intermediate value (2.5 $\mu\text{g/ml}$) was established for the theoretical analysis of CNT-nanodescriptors. This was considered reasonable because it allows the study of the nanostructure-activity relationship and at the same time considers non-agglomeration conditions for simulation of CNT-nanodescriptors in mitochondrial exposure.¹⁸ In this sense the predictions show that $^{\text{min}}D_i$ and $^{\text{max}}W_i$ are relevant nanodescriptors strongly implicated in the inhibition of mitochondrial permeability transition induced by Ca^{2+} , Fe^{2+} , H_2O_2 for carbon nanotubes. Small increments of $^{\text{min}}D_i$ including SWCNT and MWCNT may affect the function

of certain proteins and enzymes and induce serious cytotoxic effects at the biochemical and/or sub-cellular level as we assayed in the isolated mitochondria experimental model. Theoretical predictions model the variations of carbon nanotubes diameter ($0\% < {}^{\text{min}}D_i < 10\%$) associated with mitochondrial dysfunction (swelling). The results suggest that larger diameters also could act blocking or interfering with the function of carriers and mitochondrial proteins which forms MPTP (like VDAC and ANT) and in this way inhibit apoptosis through deficient MPTP assembly in swelling experimental conditions.

On the other hand the theoretical predictions to increase the functionalization ($0\% < {}^{\text{max}}W_i < 10\%$) reveals interesting aspects about the relationship nanostructure-mitoprotective activity (MPT-inhibitors) of oxidized carbon nanotubes family particularly related to motif structure in order (carboxylated-motif) > (hydroxylated-motif) and considering the walls number of CNT (MW-motif) > (SW-motif) in pro-oxidant conditions against mitochondrial swelling in order (swelling assays induced by Fe^{2+} ; P_2) > (swelling assay induced by H_2O_2 ; P_3), suggesting mechanisms based on the inhibition of Fenton-Haber-Weiss reaction.

Table 8 comes about here

Conclusions

The prediction of relationships between carbon nanomaterials physic-chemical properties and biological responses, has gained a significant importance to reduce their toxic effects and extend their nanotechnology applications. The structural determinants for mitochondrial mechanisms of functionalized CNTs (oxidized) are remaining poorly understood actually. We found that the CNTs-COOH and CNT-OH were more biocompatibility compared with the p-MWCNTs to prevent the mitochondrial dysfunction.

We can use mixed experimental-theoretic methodology to study the effects of different CNT in the modulation of mitochondrial permeability transition pore under the influence of multiple factors. In this context the modulation of mitochondrial physiology through MPTP in experimental swelling condition (Ca^{2+} , Fe^{2+} , H_2O_2 overload) using oxidized CNT can represent a qualitative advance in the treatment of several chronic diseases (hepatotoxicity, Alzheimer, Parkinson, cardiac ischemia) where MPTP has been directly involved.

Particularly NQSPR perturbation approach used here can contribute to predict nanotoxicological data allowing to infer the effects of new nanomaterials in a short time. Indeed, the derived nano-QSTR perturbation model to mitochondrial swelling provided new insights regarding the typical CNT-nanodescriptors (length, diameter, shape, partition coefficient, chemical functionalization, solubility and Young's modulus) related to mitochondrial responses as therapeutic target at the sub-cellular level, as well as the influence of different experimental conditions under which these physico-chemical properties were evaluated. Finally this *in silico* method allows the prediction of the potential mitoprotective effects of several nanoparticles under conditions not tested in our original database, which could be used to make regulatory decisions, rational design of CNT more selective and less mitotoxic.

Acknowledgements

M. González-Durruthy acknowledges Doctoral fellowship (Post-graduate Students Program PEC-PG No.062/2013) from Brazilian Agencies CAPES-CNPq. J.M. Monserrat is a productivity fellow from CNPq (PQ 307880/2013-3). This study was supported with funds from Brazilian CNPq (Project numbers 552131/2011-3, 479053/2012-0 and 452088/2015-1) given to J. M. Monserrat.

References

1. R. A Haworth and D.R Hunter, *Arch Biochem Biophys.*, **1979**, 195, 460-467.
2. L. Dong-Wei, H. Huan, L. Bing-Bing, X. Zi-Qiang, J. Feng-Lei, L. Liu. *RSC Adv.*, **2014**, 4, 3913–3919.
3. Z. Jie, Z. Zhi-Qiang, J. Jian-Cheng, Y. Lian, H. Huan, J. Feng-Lei, Y. Xiao-Gang, D. Jie, L. Yi. *Chemosphere.*, **2014**, 100, 194–199.

4. G. Jia-ling, W. Man, W. Xuan, Z. Ye-Zhong, J. Feng-Lei, L. Yi, D. Jie. *J Membrane Biol.*, **2015**, 248,39–46.
5. X. Cai-Fen, L. Long, C. Xin-You, F. Bo-Qiao, L. Ke-Lin, Q. Cai-Qin, L. Yi. *J Membrane Biol.*, **2015**,248,319–326.
6. P.A. de Faria, F. Bettanin, E. Paredes-Gamero, I.L. de-Mello, T. Nantes and T. Rodrigues, *Toxicol.*, **2015**, 330, 44-54.
7. C.T. Tan, T.Y. Saw, C.W. Fong and H.K. Ho, *Redox Biol.*, **2015**, 4, 308-320.
8. A. Shvedova, A. Pietroiusti, B. Fadeel and V.E. Kagan., *Toxicol App Pharmacol* **2012**, 261, 121–133.
9. X. Wang, J. Guo, T. Chen, T.H Nie, H. Wang, J. Zang, X. Cui and G. Jia, *Toxicol. In Vitro*, **2012**, 26, 799-806.
10. S. Ye, Y. Jiang, H. Zhang, Y. Wang, Y. Wu, Z. Hou and Q. Zhang, *J. Nanosci. Nanotechnol.*, **2012**, 12, 2101-12.
11. M. Garcia-Fuentes, H. Gonzalez-Diaz and N. Csaba, *Curr. Top. Med. Chem.*, **2014**, 14, 1095-6.
12. R. Tantra, C. Oksel, T. Puzyn, J. Wang, K.N. Robinson, X.Z Wang, C.Y. Ma and T. Wilkins, *Nanotoxicology*, **2014**, 1, 1-7.
13. A. Gajewicz, N. Schaeublin, B. Rasulev, S. Hussain, D. Leszczynska, T. Puzyn, and J. Leszczynski, *Nanotoxicology*, **2014**, 1, 1-13.
14. S. Kar, A. Gajewicz, T. Puzyn and K. Roy, *Toxicol. In Vitro*, **2014**, 28, 600-6.
15. A.A. Toropov, A.P. Toropova, T. Puzyn, E. Benfenati, G. Gini, D. Leszczynska and J. Leszczynski, *Chemosphere*, **2013**, 92, 31-7.
16. A. A. Toropov, A.P. Toropova, E. Benfenati, G. Gini, T. Puzyn, D. Leszczynska and J. Leszczynski, *Chemosphere*, **2012**, 89, 1098-102.
17. T. Puzyn, B. Rasulev, A. Gajewicz, X. Hu, T.P. Dasari, A. Michalkova, H.M Hwang, A. Toropov, D. Leszczynska and J. Leszczynski, *Nat. Nanotechnol.*, **2011**, 6, 175-8.
18. B. D. Shane, S. Zhenyu, S. Philip, H. James, N.C. Jonathan, *J. Phys. Chem. C* **2010**, 114, 231–237
19. N. Sizochenko, B. Rasulev, A. Gajewicz, V. Kuzmin, T. Puzyn and J. Leszczynski, *Nanoscale* **2014**, 6, 13986-93.
20. R. Carbo-Dorca and E. Besalu, *Environ. Res.*, **2011**, 22, 661-5.
21. C.Y. Shao, S. Z Chen, B.H. Su, Y.J. Tseng, E.X. Esposito and A.J. Hopfinger, *J. Chem. Inf. Model*, **2013**, 53, 142-158.
22. A.P. Toropova and A. A. Toropov, *Mini Rev. Med Chem*, **2015**, 15, 608-621.
23. A.P. Toropova, A. A Toropov and E. Benfenati, *Environ Res.*, **2015**, 26, 29-40.
24. C. Oksel, C.Y. Ma and X.Z. Wang, *Environ. Res.*, **2015**, 26, 79-94.
25. M. Shahbazy, M. Kompany-Zareh and M.M. Najafpour, *J. Photochem Photobiol. B.*, **2015**, <http://dx.doi.org/10.1016/j.jphotobiol.2014.12.020>
26. A. Gajewicz, M.T Cronin, B. Rasulev, J. Leszczynski and T. Puzyn, *Nanotechnology*, **2015**, 26:015701. doi: 10.1088/0957-4484/26/1/015701.
27. A.P. Toropova, A. A. Toropov, R. Rallo, D. Leszczynska and J. Leszczynski, *Ecotoxicol. Environ. Saf.*, **2015**, 112, 39-45.
28. A.P. Toropova, A.A. Toropov, E. Benfenati, R. Korenstein, D. Leszczynska and J. Leszczynski, *Environ. Sci. Pollut. Res. Int.*, **2015**, 22, 745-57.
29. E. Burello and A.P. Worth, *Interdis. Rev. Nanomed. Nanobiotechnol.*, **2011**, 3, 298-306.
30. C. Hansch, D. Hoekman, A. Leo, D. Weininger and C.D. Selassie, *Chem Rev.*, **2002**, 102, 783-812.
31. C. Hansch, A. Kurup, R. Garg and H. Gao, *Chem. Rev.*, **2001**, 101, 619-72.
32. C. Hansch, W.E. Steinmetz, A.J. Leo, S.B. Mekapati, A. Kurup and D. Hoekman, *J. Chem. Inf. Comput. Sci.*, **2003**, 43, 120-5.
33. H. Gonzalez-Diaz, S. Arrasate, A. Gomez-San Juan, N. Sotomayor, E. Lete, L. Besada-Porto and J.M. Ruso, *Curr. Top. Med. Chem.*, **2013**, 13, 1713-41.

34. H. Gonzalez-Diaz, S. Arrasate, A.G. Juan, N. Sotomayor, E. Lete, A. Speck-Planche, J. M. Ruso, F. Luan and M. Cordeiro, *Curr. Drug Metab.*, **2014**, 15, 470-88.
35. J. Vergara-Galicia, F.J. Prado-Prado, H. Gonzalez-Diaz and Galvez-Markov, *Curr. Drug Metab.*, **2014**, 15, 557-64.
36. F. Luan, V.V. Kleandrova, H. Gonzalez-Diaz, J.M. Ruso, A. Melo, A. Speck-Planche and M.N. Cordeiro, *Nanoscale*, **2014**, 6, 10623-30.
37. V.V. Kleandrova, F. Luan, H. Gonzalez-Diaz, J.M. Ruso, A. Speck-Planche and M.N. Cordeiro, *Environ. Sci. Technol.*, **2014**, 48, 14686-94.
38. V.V. Kleandrova, F. Luan, H. Gonzalez-Diaz, J.M. Ruso, A. Melo, A. Speck-Planche and M.N. Cordeiro, *Environ. Int.*, **2014**, 73, 288-94.
39. A. Speck-Planche, V.V. Kleandrova, F. Luan and M.N. Cordeiro, *Nanomed.*, **2015**, 10, 193-204.
40. P.L. Pedersen, J.W. Greenawalt, B. Reynafarje, J. Hullihen, G.L. Decker, J.W. Soper and E. Bustamente, *Methods Cell. Biol.*, **1978**, 20, 411-81.
41. G.L. Pardo-Andreu, Y. Nunez-Figueroa, V.G. Tudella, O. Cuesta-Rubio, F. P. Rodrigues, C.R. Pestana, S.A. Uyemura, A.M. Leopoldino, L.C. Alberici and C. Curti, *Toxicol. Appl. Pharmacol.*, **2011**, 253, 282-289.
42. B.V. Chernyak, V.N. Dedov and V. Chernyak, *FEBS Lett.*, **1995**, 365, 75-8.
43. G.L. Pardo-Andreu, R. Delgado, J.A. Velho, C. Curti and A.E. Vercesi, *Arch. Biochem. Biophys.*, **2005**, 439, 184-93.
44. D. Jia-Xin, Z. Guang-Yuan, Y. Qiu-Li-Yang, L. Ran, Y. Lian, C. Jing, L. Yi. *J Membrane Biol.*, **2013**, 246, 375-381.
45. L. Jia-han, L. Xiao-rong, Z. Yue, T. Fang-fang, Z. Guang-yuan, Y. Qiu-li-yang, J. Feng-lei, L. Yi. *Toxicol Res.*, **2012**, 1, 137-144.
46. G.L. Pardo-Andreu, R. Delgado, A.J. Nunez-Selles and A.E. Vercesi, *Pharmacol. Res.*, **2006**, 53, 253-260.
47. L. Jiahan, Z. Yue, X. Qi, T. Fangfang, L. Xiaorong, L. Ran, Z. Guangyuan, J. Fenglei, L. Yi. *J. Hazardous Materials.*, **2011**, 194, 440-444.
48. Z. Yue, T. Fangfang, X. Qi, H. Yanjun, L. Jiahan, J. Fenglei, L. Yi. *J. Membrane Biol.*, **2013**, 246, 365-373.
49. M. Reers, T.W. Smith and L.B. Chen., *Biochem*, **1991**, 30, 4480-4486.
50. T. Hill, P. Lewicki. *Statistics: Methods and Applications: a Comprehensive Reference for Science, Industry, and Data Mining*, ISBN: 1884233597, StatSoft, Inc., 2006, pp. 832.
51. K. Chan, D. Truong, N. Shangari and P.J. O'Brien. *Expert Opin. Drug Metab. Toxicol.*, **2005**, 4, 655-669.
52. M. Xiaowei, Z. Li-Hua, W. Li-Rong, X. Xue, S. Ji-Hong, W. Yan, Z. Guozhang, W. Xia, W. C Paul, G.W. Wayne, Y. Jun-Jie, Z. Kaiyuan, L. Xing-Jie, *ACS Nano.*, **2012**, 12, 10486-10496.
53. G.L. Andreu, R. Delgado, J.A. Velho, C. Curti and A.E. Vercesi, *Eur. J. Pharmacol.*, **2005**, 513, 47-55.
54. V. Giorgio, M.E. Soriano, E. Basso, E. Bisetto, G. Lippe, M.A. Forte and P. Bernardi, *Biochim. Biophys. Acta*, **2010**, 1797, 1113-1118.
55. V.M. Figueredo, K.P. Dresdner, A.C. Wolney and A.M. Keller, *Cardiovasc. Res.*, **1991**, 25, 337-342.
56. A.A. Toropov, D. Leszczynska and J. Leszczynski, *Comput. Biol. Chem.*, **2007**, 31, 127-128.
57. H.H. Vilela-Costa, G.F. Lima, L.R. Nacano and C.R.T. Tarley, *Wat. Air Soil Pollut.*, **2011**, 217, 557-565.
58. L. Zhenbao, L. Yanfei, P. Dongming. *J. Biomed Mat.* **2015**. DOI: 10.1002/jbm.a.35416
59. C. Yong, Q. Konggang, Z. Chuanqi, W. Li, R. Jinsong, W. Jiasi, Q. Xiaogang. *Nat Comms.*, **2012**, doi: 10.1038/ncomms2091.
60. A.P. Halestrap and C. Brenner, *Curr. Med. Chem.*, **2003**, 10, 1507-1525.

61. G.J. Gores, C.E. Flarsheim, T.L. Dawson, A.L. Nieminen, B. Herman and J.J. Lemasters, *Biochim. Biophys. Acta*, **2006**, 1762, 181–190.
62. F. Di Lisa, A. Carpi, V. Giorgio and P. Bernardi, *Biochim. Biophys. Acta*, **2011**, 1813, 1316–1322
63. M. Colombini, *Mol. Cell. Biochem*, **2004**, 256–257, 107–115.
64. A. Masini, D. Ceccarelli, F. Giovannini, G. Montosi, C. Garuti and A. Pietrangelo, *J. Bionerg. Biomembr*, **2000**, 32, 175–182.
65. A. Pietrangelo, G. Montosi, C. Garuti, M. Contri, F. Giovannini, D. Ceccarelli and A. Masini, *J. Bionerg. Biomembr.*, **2002**, 34, 67–79.
66. U. Rauen, F. Petrat, R. Sustmann and H. Groot, *J. Hepatol.*, **2004**, **40**, 607–615.
67. D. Ashton, J. van Reempts and A. Wauquier, *Arch. Pharmacol. Ther.*, **1981**, 254, 196–213.
68. G.L. Pardo-Andreu, R. Delgado, A.J. Núñez-Sellés and A.E. Vercesi, *Pharmacol. Res.*, **2006**, 53, 253–260.
69. H. Dumortier, S. Lacotte, G. Pastorin, R. Marega, W. Wu, D. Bonifazi, J.P. Briand, M. Prato, S. Muller and A. Bianco, *Nano Lett.*, **2006**, 6, 1522–1528.
70. A. Toninello, P. Pietrangeli, U. De Marchi, M. Salvi and B. Mondovì, *Biochim. Biophys. Acta*, **2009**, **178**, 1425–1432.
71. J. Wang, S. Pingping, B. Yongming, D. Bairui, S. Dandan and L. Yachen, *Toxicol. in Vitro*, **2012**, 26, 32–41.
72. A. Karakoti, S. Singh, J.M. Dowding and S. Seal, *Chem. Soc. Rev.*, **2010**, 39, 4422–4432.
73. A. Albin, V. Mussi, A. Parodi, A. Ventura, E. Principi, *Nanotech Biol Med*, **2010**, 6, 277–288.
74. Z. Yang, Y. Zhang, Y. Yang, L.H. Dong, H. Li, C. Wang, *Nanomed: Nanotech Biol Med*, **2010**, 6, 427–441.
75. J.J. Liao, R. Liu, *J. Chemometrics*, **2009**, 23, 248–253.
76. P.G. Gottschalk and J.R. Dunn, *Anal Biochem.*, **2005**, 343, 54–65.
78. E. Tenorio-Borroto, F.R. Ramirez, A. Speck-Planche, M.N. Cordeiro, F. Luan and H. Gonzalez-Diaz, *Curr. Drug Metab.*, **2014**, 15, 414–428.
79. E. Tenorio-Borroto, C.G. Peñuelas-Rivas, J.C. Vásquez-Chagoyán, N. Castañedo, F.J. Prado-Prado, X. García-Mera and H. González-Díaz. *Eur. J. Med. Chem.*, **2014**, 72, 206–20.

FIGURES TO BE INSERTED

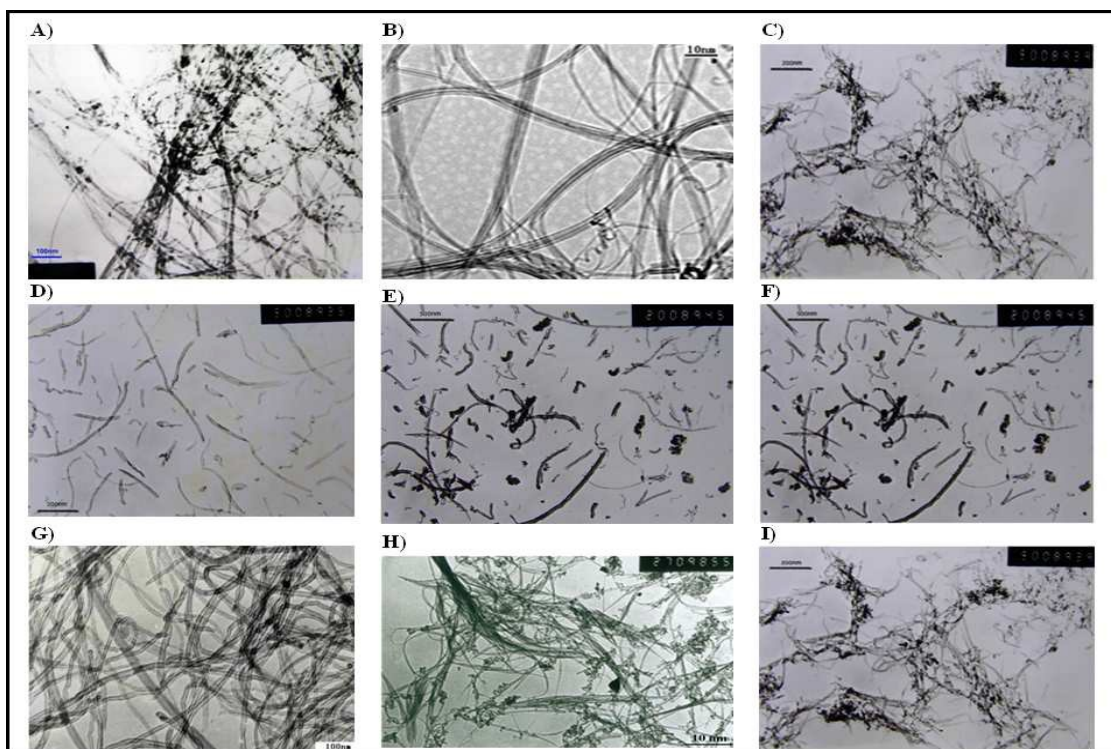


Figure 1. TEM images of carbon nanotubes used in this study. a) pristine-MWCMT [CNT1], b) SW/DWCNT-OH [CNT2], c) MWCNT-OH [CNT3], d) MWCNT-OH [CNT4], e) MWCNT-OH [CNT5], f) MWCNT-COOH [CNT6], g) MWCNT-COOH [CNT7], h) SWCNT-COOH [CNT8], i) MWCNT-COOH [CNT9].(TEM, Tecnai G2-12-SpiritBiotwin FEI- 120 kV).

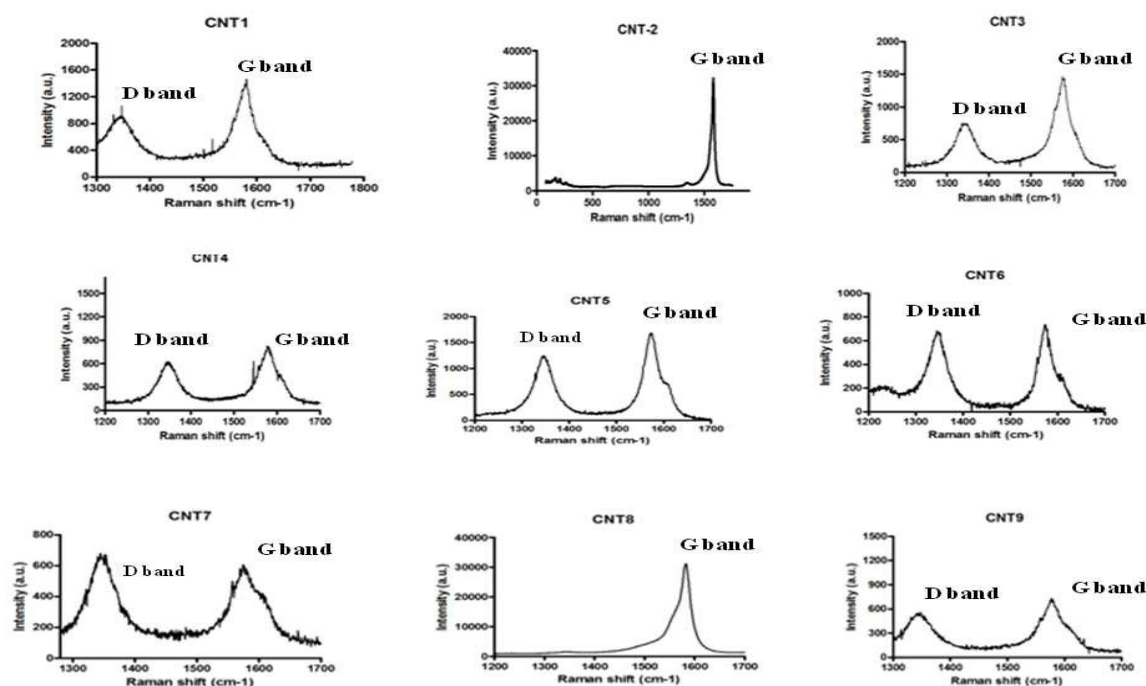


Figure 2. Raman spectra of carbon nanotubes used in this study. Pristine-MWCMT (CNT1), SW/DWCNT-OH (CNT2), MWCNT-OH (CNT3), MWCNT-OH (CNT4), MWCNT-OH (CNT5), MWCNT-COOH (CNT6), MWCNT-COOH (CNT7), SWCNT-COOH (CNT8), MWCNT-COOH (CNT9). (For more details see Materials and Methods.)

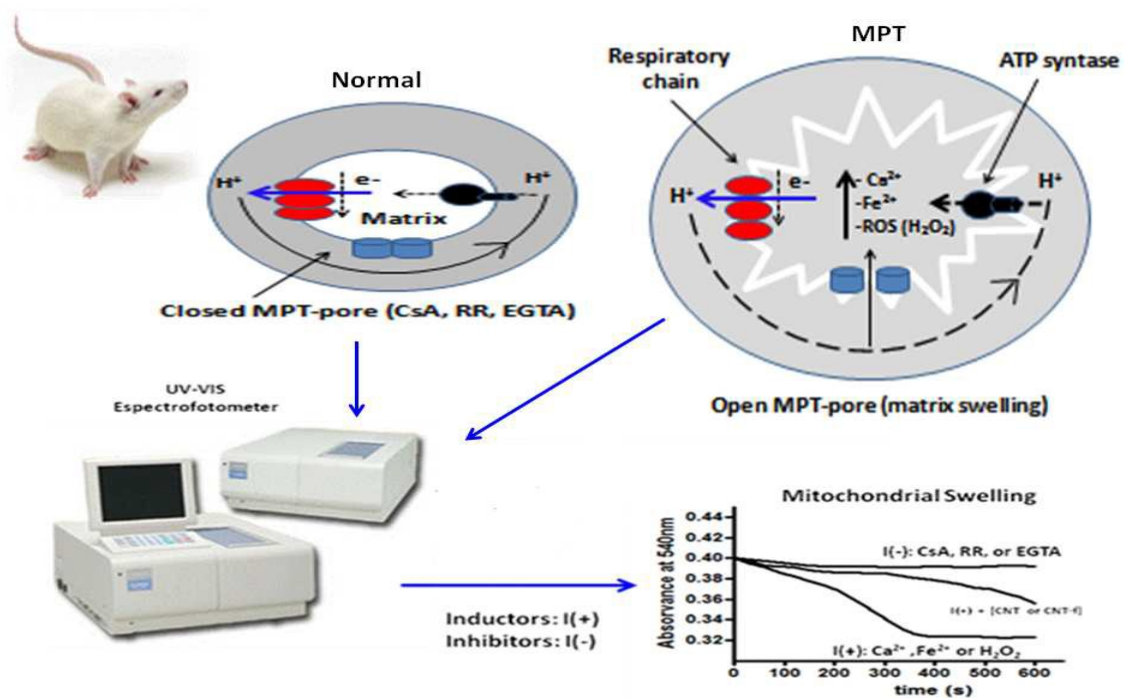


Figure 3. Workflow of the experimental section.

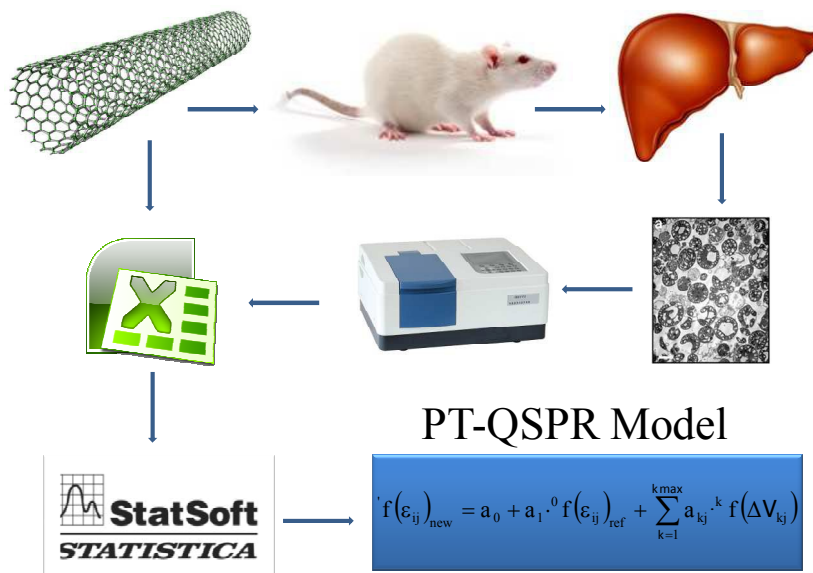


Figure 4. Workflow used here to seek the PT-QSPR models

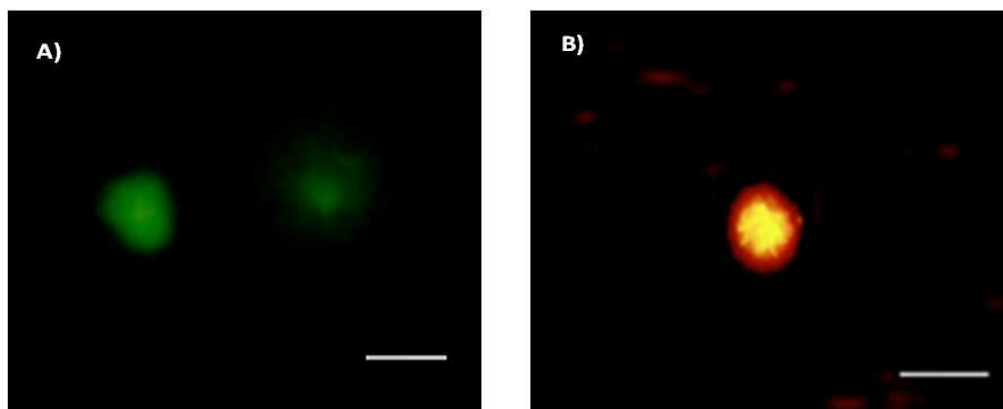
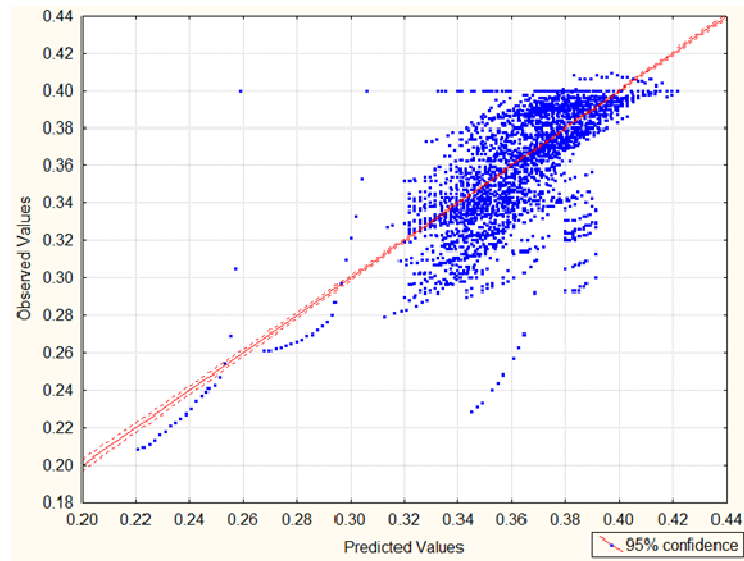


Figure 5. Isolated rat-liver mitochondria were incubated with a specific mitochondrial dye (JC-1) in 0.2 mg/ml for 15 min. Show representative fluorescent images of effects on mitochondrial membrane potential for different swelling conditions after exposure with MPT-inductor (Ca^{2+} , Fe^{2+} or H_2O_2) (A) and MPT-inhibitor (CsA, RR, EGTA or CNT-COOH > CNT-OH > pristine-CNT) (B) were examined under a fluorescence microscope (x 600 magnification). Scale bars 50 μm .

(A)



(B)

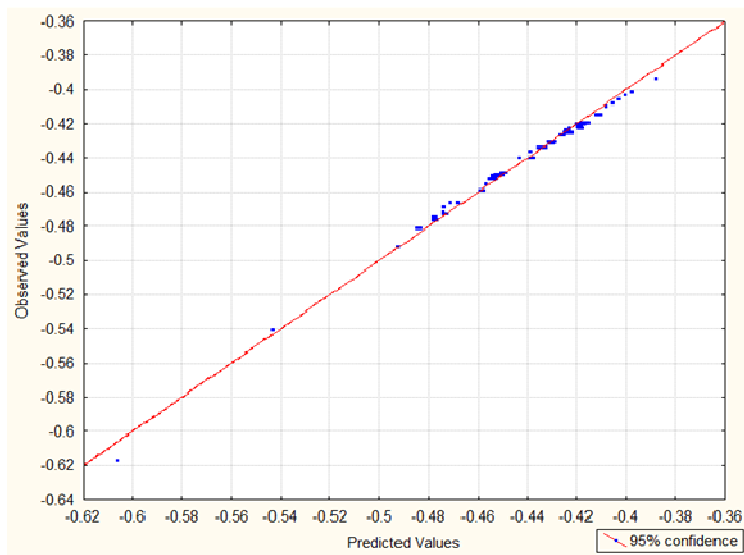


Figure 6. Observed vs. Predicted values for models with $f(\varepsilon_{ij}) = \varepsilon_{ij}$ (A), and (B) $f(\varepsilon_{ij}) = -\log(\varepsilon_{ij})$

TABLES TO BE INSERTED

Table 1. Physico-chemical parameters (kV_i) of CNT family.

CNT Properties ^a			W_i (%)		D_i (nm)		L_i	P_i	M_i	C_i
n	type	function	min	max	min	max	(μm)	(%)	(%Metal)	$\text{S}\cdot\text{cm}^{-1}$
1	MWCNT	-	0.9 ^b	3.03 ^b	8	8	0.5-2	>95	< 5	<1.5
2	SW/DWCNT	OH	0	3.96	1	4	0.5-2	>95	< 5	<1.5
3	MWCNT	OH	0	3.86	1	8	0.5-2	>95	< 5	<1.5
4	MWCNT	OH	3	4	10	20	0.5-2	>95	< 5	<1.5
5	MWCNT	OH	1	1.06	30	50	0.5-2	>95	< 5	<1.5
6	MWCNT	COOH	0	0.73	30	50	0.5-2	>95	< 5	<1.5
7	MWCNT	COOH	3	4	10	20	0.5-2	>95	< 5	<1.5
8	SWCNT	COOH	0	2.73	1	4	0.5-2	>95	< 5	<1.5
9	MWCNT	COOH	0	3.86	1	8	0.5-2	>95	< 5	<1.5

^a MWCNT = Multiple-Walled, SWCNT = Single-Walled, SW/DWCNT = DWCNT + SWCNT mixture, W_i (%) = Functional groups (OH, COOH) carbon atoms ratio (%); the properties of the i^{th} Carbon Nanotube (CNT) are D_i = CNT outer diameter, L_i = CNT Length, P_i = Purity, C_i = Electric conductivity, M_i = metal impurities.

Table 2. Description of input variables and functions

Coefficient	Input Variable	MA	Function f^k	Function examples	Information
-	-	-	f	$(\epsilon_{ij})_{new}$, $1/(\epsilon_{ij})_{new}^2$, $-\log(\epsilon_{ij})_{new}$	Predicted absorbance
e_0	-	-	-	-	Error term.
a_0	-	-	f^0	$\langle \epsilon_{ij} \rangle$	Average of value of absorbance for all CNTs samples for multiple experimental conditions (assay, CNT-type, chemical function, MPT-inductors, MPT-inhibitors).
a_1	t_{ij}	Δt_{ij}	f^1	$\Delta t_{ij}(s)$, $\exp(-\Delta t_{ij}(s))$	Exposure time.
a_2	c_{ij}	Δc_{ij}	f^2	$\Delta c_{ij}(\mu\text{g/ml})$, $1/(1+\Delta c_{ij}(\mu\text{g/ml}))$	CNT concentration.
a_3	W_i^{\max}	ΔW_{ij}	f^3	$\Delta W_{ij}(\%)_{\max}$	CNT maximum function / carbon ratio.
a_4	D_i^{\min}	ΔD_{ij}	f^4	$\Delta D_{ij}(\text{nm})_{\min}$	CNT minimum outer diameter.

Table 3. Experimental values of mitochondrial swelling induced by Ca^{2+} for CNT family

CNT ^a						Experimental mitoprotective activity vs. Ca^{2+} ^b					
n_i	type	function	W_i	D_i	c_{ij}	P_1	N_j	P_2	N_j	P_3	N_j
1	MWCNT	-	3.03 ^b	8	0.5	0	42	0	42	0	42
					1	3.5	42	3.4	42	4.1	42
					3	0	42	0	42	0	42
					5	32.3	42	31.2	42	37.8	42
2	SW/DWCNT	OH	3.96	1	0.5	0	21	0	21	0	21
					1	0	21	0	21	0	21
					3	31.9	21	30.7	21	37.3	21
					5	60.7	21	58.5	21	71.0	21
3	MWCNT	OH	3.86	1	0.5	8.3	42	8.0	42	9.8	42
					1	17.3	42	16.7	42	20.3	42
					3	7.3	42	7.1	42	8.6	42
					5	20.2	42	19.5	42	23.7	42
4	MWCNT	OH	4	10	0.5	0	21	0	21	0	21
					1	0	21	0	21	0	21
					3	0	21	0	21	0	21
					5	0	21	0	21	0	21
5	MWCNT	OH	1.06	30	0.5	0	42	0	42	0	42
					1	0	42	0	42	0	42
					3	0	42	0	42	0	42
					5	6.4	42	6.2	42	7.5	42
6	MWCNT	COOH	0.73	30	0.5	10.6	21	10.2	21	12.4	21
					1	0	21	0	21	0	21
					3	0	21	0	21	0	21
					5	0	21	0	21	0	21
7	MWCNT	COOH	4	10	0.5	0	21	0	21	0	21
					1	0	21	0	21	0	21
					3	66.9	21	64.5	21	78.2	21
					5	71.2	21	68.7	21	83.3	21
8	SWCNT	COOH	2.73	1	0.5	0	21	0	21	0	21
					1	0	21	0	21	0	21
					3	22.9	21	22.1	21	26.8	21
					5	67.3	21	64.9	21	78.7	21
9	MWCNT	COOH	3.86	1	0.5	0	21	0	21	0	21
					1	0	21	0	21	0	21
					3	75.9	21	73.2	21	88.8	21
					5	81.4	21	78.5	21	95.2	21
	Groups		W_i	D_i	c_{ij}	e_{ij}	N_j	e_{ij}	N_j	e_{ij}	N_j
	IC+S	Average	2.435	10.25	2.5	0.353	1071	0.353	1071	0.353	1071
		± SD				0.000		0.000		0.000	
	TC+IC+S	Average				0.395	63	0.397	63	0.389	63
		± SD				0,0075		0.001		0.0079	

^a MWCNT = Multiple-Walled, SWCNT = Single-Walled, SW/WCNT = MWCNT + SWCNT mixture. ^b Mitoprotective activity, P (%) = $100 \cdot [\varepsilon_{ij}(\text{CNT} + \text{TC} + \text{S})_{\text{obs}} - \varepsilon_{ij}(\text{TC} + \text{S})_{\text{obs}}] / [\varepsilon_{ij}(\text{IC} + \text{TC} + \text{S})_{\text{obs}} - \varepsilon_{ij}(\text{TC} + \text{S})_{\text{obs}}]$ and N_j is the number of replicates of

the assay. CNT = Carbon nanotube, TC = Toxic control (MPT-inductor), IC = Inhibitor control (MPT-inhibidor), S = Solvent. The details of the assays are the following: for toxicity assay P₁ (a = 1), TC = Ca²⁺, IC = CsA, and Solvent = DMSO, for assay P₂ (a = 2) TC = Ca²⁺, IC = EGTA and Solvent = DMSO; and for assay P₃ (a = 3), TC = Ca²⁺, IC = RR, and Solvent = DMSO.

Table 4. Experimental values of mitochondrial swelling induced by Fe²⁺ for CNT family

CNT _i ^a						Experimental mitoprotective activity vs. Fe ²⁺ ^b					
n _i	type	function	W _i	D _i	c _{ij}	P ₁	N _j	P ₂	N _j	P ₃	N _j
1	MWCNT	-	3.03 ^b	8	0.5	0	14	0	14	0	14
					1	0	14	0	14	0	14
					3	0	16	0	16	0	16
					5	20.3	14	90.8	14	0	14
2	SW/DWCNT	OH	3.96	1	0.5	0	14	0	14	0	14
					1	35.3	14	100	14	0	14
					3	84.8	16	100	16	0	16
					5	100	14	100	14	67.2	14
3	MWCNT	OH	3.86	1	0.5	0	14	42.5	14	0	14
					1	0	14	79.4	14	0	14
					3	93.3	16	100	16	0	16
					5	92.5	14	100	14	0	14
4	MWCNT	OH	4	10	0.5	0	14	0	14	0	14
					1	44.4	14	100	14	0	14
					3	100	16	100	16	0	16
					5	100	14	100	14	10.7	14
5	MWCNT	OH	1.06	30	0.5	0	14	0	14	0	14
					1	0	14	0	14	0	14
					3	0	16	0	16	0	16
					5	6.8	14	30.2	14	0	14
6	MWCNT	COOH	0.73	30	0.5	0	14	68.4	14	0	14
					1	0	14	14.7	14	0	14
					3	0	16	16.9	16	0	16
					5	80.4	14	100	14	0	14
7	MW	COOH	4	10	0.5	12.0	14	53.8	14	0	14
					1	91.0	14	100	14	0	14
					3	100	16	100	16	0	16
					5	100	14	100	14	0	14
8	SWCNT	COOH	2.73	1	0.5	0	14	0	14	0	14
					1	37.6	14	100	14	0	14
					3	90.7	16	100	16	0	16
					5	100	14	100	14	2.3	14
9	MW	COOH	3.86	1	0.5	0	14	0	14	0	14
					1	30.8	14	100	14	0	14
					3	100	16	100	16	0	16
					5	100	14	100	14	24.8	14
	Groups		<W _i >	<D _i >	<c _{ij} >	<e _{ij} >	N _j	<e _{ij} >	N _j	<e _{ij} >	N _j
	IC+S	Average	2.435	10.25	2.5	0.393	189	0.378	189	0.337	126
		± SD				0.000		0.000		0.000	

	TC+IC+S	Average				0.374	781	0.374	781	0.374	781
		± SD				0.003		0.001		0.030	

^a MWCNT = Multiple-Walled, SWCNT = Single-Walled, SW/WTCNT = MWCNT + SWCNT mixture. ^b Mitoprotective activity, $P (\%) = 100 \cdot [\varepsilon_{ij}(\text{CNT} + \text{TC} + \text{S})_{\text{obs}} - \varepsilon_{ij}(\text{TC} + \text{S})_{\text{obs}}] / [\varepsilon_{ij}(\text{IC} + \text{TC} + \text{S})_{\text{obs}} - \varepsilon_{ij}(\text{TC} + \text{S})_{\text{obs}}]$ and N_j is the number of replicates of the j^{th} assay. CNT = Carbon nanotube, TC = Toxic control (MPT-inductor), IC = Inhibitor control (MPT-inhibitor), S = Solvent. The details of the assays are the following: Assay P₁ (a = 1) TC₁ = Fe²⁺, IC = EGTA and S = DMSO; Assay P₂ (a = 3), TC₁ = Fe²⁺, TC₂ = KCN, IC = EGTA and Solvent = DMSO and Assay P₃ (a = 3), TC₁ = Fe²⁺, TC₂ = VitC, IC = EGTA and Solvent = DMSO.

Table 5. Experimental values of mitochondrial swelling induced by H₂O₂ for CNT family

CNT ^a						Experimental mitoprotective activity vs. H ₂ O ₂ ^b					
n _i	Type	Function	W _i	D _i	c _{ij}	P ₁	N _j	P ₂	N _j	P ₃	N _j
1	MWCNT	-	3.03 ^b	8	0.5	0	0	0	0	0	0
					1	0	7	0	7	0	7
					3	0	7	0	7	0	7
					5	0	7	100	7	0	7
2	SW/DWCNT	OH	3.96	1	0.5	0	0	0	0	0	0
					1	0	21	65	21	0	21
					3	100	21	80	21	0	21
					5	100	21	81.0	21	72.7	21
3	MWCNT	OH	3.86	1	0.5	0	0	0	0	0	0
					1	100	21	95	21	0	21
					3	100	21	97	21	0	21
					5	100	21	97.5	21	98.0	21
4	MWCNT	OH	4	10	0.5	0	0	0	0	0	0
					1	100	21	51	21	0	21
					3	100	21	97.5	21	0	21
					5	100	21	95.5	21	100	21
5	MWCNT	OH	1.06	30	0.5	0	0	0	0	0	0
					1	100	21	95	21	0	21
					3	100	21	97	21	0	21
					5	100	21	97.5	21	100	21
6	MWCNT	COOH	0.73	30	0.5	0	0	0	0	0	0
					1	100	21	51	21	0	21
					3	100	21	97	21	0	21
					5	100	21	97.5	21	91.0	21
7	MWCNT	COOH	4	10	0.5	0	0	0	0	0	0
					1	100	21	80	21	0	21
					3	100	21	81	21	0	21
					5	100	21	91	21	100	21
8	SWCNT	COOH	2.73	1	0.5	0	0	0	0	0	0
					1	100	21	80	21	0	21
					3	100	21	81	21	0	21
					5	100	21	91	21	90.2	21
9	MWCNT	COOH	3.86	1	0.5	0	0	0	0	0	0
					1	100	21	86	21	0	21
					3	100	21	97	21	0	21
					5	100	21	95.5	21	100	21
	Groups		<W _i >	<D _i >	<c _{ij} >	<e _{ij} >	N _j	<e _{ij} >	N _j	<e _{ij} >	N _j
	IC+S	Average	2.435	10.25	2.5	0.366	175	0.404	175	0.241	105
		± SD				0.000		0.000		0.000	
	TC+IC+S	Average				0.375	525	0.375	525	0.375	525
		± SD				0.001		0.006			0.00

						5		8		
--	--	--	--	--	--	---	--	---	--	--

^a MWCNT = Multiple-Walled, SWCNT = Single-Walled, SW/WTCNT = MWCNT + SWCNT mixture. ^b Mitoprotective activity, $P (\%) = 100 \cdot [\varepsilon_{ij}(\text{CNT}+\text{TC}+\text{S})_{\text{obs}} - \varepsilon_{ij}(\text{TC}+\text{S})_{\text{obs}}] / [\varepsilon_{ij}(\text{IC}+\text{TC}+\text{S})_{\text{obs}} - \varepsilon_{ij}(\text{TC}+\text{S})_{\text{obs}}]$ and N is the number of replicates of the assay. CNT = Carbon nanotube, TC = Toxic control (MPT-inductor), IC = Inhibitor control (MPT-inhibitor), S = Solvent. The details of the assays are the following: Assay P₁ (a = 1) TC₁ = H₂O₂, IC = Q and Solvent = DMSO; Assay P₂ (a = 2), TC₁ = H₂O₂, IC = CsA, and Solvent = DMSO; Assay P₃ (a = 2), TC₁ = H₂O₂, TC₂ = Fe²⁺, IC = Q, and Solvent = DMSO.

Table 6. Statistical analysis for alternative PT-NQSPR models developed in this work

Model Parameters					Model			
V _k	a _k	s.e.	t	p	Specifications			
a ₀	-0.000780	0.003041	-0.26	0.79	Model 1			
<ε _{ij} >	1.002419	0.008302	120.75	0.00	¹ f(ε _{ij})	⁰ f(ε _{ij})	¹ f(t _{ij})	² f(c _{ij})
Δt _{ij}	-0.000066	0.000002	-42.77	0.00	ε _{ij}	<ε _{ij} >	Δt _{ij}	Δc _{ij}
Δc _{ij}	0.002395	0.000199	12.02	0.00	R ²	F	p	q ²
ΔW _{max}	-0.001175	0.000237	-4.97	0.00	0.73	3308.1	< 0.05	0.70
ΔD _{min}	-0.000735	0.000174	-4.21	0.00				
a ₀	0.92771	0.000488	-1900.43	0.00	Model 2			
<ε _{ij} >	-1.33764	0.001332	1003.91	0.00	¹ f(ε _{ij})	⁰ f(ε _{ij})	¹ f(t _{ij})	² f(c _{ij})
Δt _{ij}	0.00001	0.000000	-2.02	0.04	-log(ε _{ij})	<ε _{ij} >	Δt _{ij}	Δc _{ij}
Δc _{ij}	-0.00038	0.000032	11.92	0.00	R ²	F	p	q ²
ΔW _{max}	-0.00042	0.000038	11.11	0.00	0.994	203384.0	< 0.05	0.994
ΔD _{min}	-0.00044	0.000028	15.79	0.00				
a ₀	32.5709	0.190990	170.53	0.00	Model 3			
<ε _{ij} >	-67.6535	0.521307	-129.78	0.00	¹ f(ε _{ij})	⁰ f(ε _{ij})	¹ f(t _{ij})	² f(c _{ij})
Δt _{ij}	0.0035	0.000096	36.33	0.00	1/(ε _{ij}) ²	<ε _{ij} >	Δt _{ij}	Δc _{ij}
Δc _{ij}	-0.1744	0.012517	-13.93	0.00	R ²	F	p	q ²
ΔW _{max}	-0.0111	0.014857	-0.75	0.45	0.75	3647.4	< 0.005	-
ΔD _{min}	-0.0295	0.010953	-2.69	0.01				
a ₀	6.5064	0.028482	228.44	0.00	Model 4			
<ε _{ij} >	-10.2097	0.077742	-131.33	0.00	¹ f(ε _{ij})	⁰ f(ε _{ij})	¹ f(t _{ij})	² f(c _{ij})
Δt _{ij}	0.0006	0.000014	39.71	0.00	1/ε _{ij}	<ε _{ij} >	Δt _{ij}	Δc _{ij}
Δc _{ij}	-0.0259	0.001867	-13.86	0.00	R ²	F	p	q ²
ΔW _{max}	0.0027	0.002216	1.20	0.23	0.76	3780.1	< 0.05	-
ΔD _{min}	-0.0003	0.001633	-0.20	0.84				
a ₀	0.002922	0.003037	0.96	0.33	Model 5			
<ε _{ij} >	0.998287	0.008275	120.63	0.00	¹ f(ε _{ij})	⁰ f(ε _{ij})	¹ f(t _{ij})	² f(c _{ij})
Δt _{ij}	-0.000060	0.000002	-39.37	0.00	ε _{ij}	<ε _{ij} >	Δt _{ij}	1/(1+Δc _{ij})
Δc _{ij}	-0.000467	0.000207	-2.25	0.02	R ²	F	p	q ²
ΔW _{max}	-0.000420	0.000166	-2.53	0.01	0.734	3331.7	< 0.05	-
ΔD _{min}	-0.006490	0.000488	-13.29	0.00				
a ₀	-0.927407	0.000494	-1877.49	0.00	Model 6			
<ε _{ij} >	1.337072	0.001346	993.49	0.00	¹ f(ε _{ij})	⁰ f(ε _{ij})	¹ f(t _{ij})	² f(c _{ij})
Δt _{ij}	0	0	0.47	0.64	log(ε _{ij})	<ε _{ij} >	Δt _{ij}	1/(1+Δc _{ij})
Δc _{ij}	0.000634	0.000034	18.80	0.00	R ²	F	p	q ²
ΔW _{max}	0.000539	0.000027	19.96	0.00	0.993	199112.8	< 0.05	-

ΔD_{\min}	-0.000286	0.000079	-3.60	0.00					
-------------------	-----------	----------	-------	------	--	--	--	--	--

^a $\langle \epsilon_{ij} \rangle_{\text{ref}} = \langle \epsilon_{ij} \rangle$ is the average of ϵ_{ij} (expected value of absorbance) for a given assay carried out under the conditions b_j . ^b Symbols of input variables used. The parameters $\Delta V_{kj} = ({}^k V_i - \langle V_{kj} \rangle)$ are PT operators in form of Moving Averages, for more details see Materials and Methods.

Table 7. Expected values of variables in different conditions

Experimental conditions					Expected Values				
Type	Function	CT ₁	CT ₂	IC	$\langle \epsilon_{ij} \rangle$	$\langle V_1 \rangle$	$\langle V_2 \rangle$	$\langle V_3 \rangle$	$\langle V_4 \rangle$
MWCNT	NO	Ca ²⁺	NO	NO	0.3528	300	2.38	0	8
SW/DWCNT	OH	Ca ²⁺	NO	NO	0.3528	300	2.38	3.96	1
MWCNT	OH	Ca ²⁺	NO	NO	0.3528	300	2.38	2.97	13.67
MWCNT	COOH	Ca ²⁺	NO	NO	0.3528	300	2.38	2.86	13.67
SWCNT	COOH	Ca ²⁺	NO	NO	0.3528	300	2.38	2.73	1
MWCNT	NO	Fe ²⁺	NO	NO	0.3741	94.14	2.4	0	8
SW/DWCNT	OH	Fe ²⁺	NO	NO	0.3741	94.14	2.4	3.96	1
SW/DWCNT	OH	Fe ²⁺	VitC	NO	0.3361	90	5	3.96	1
MWCNT	OH	Fe ²⁺	NO	NO	0.3741	93.83	2.22	2.83	14.88
MWCNT	OH	Fe ²⁺	VitC	NO	0.3361	90	5	2.97	13.67
MWCNT	COOH	Fe ²⁺	NO	NO	0.3741	94.14	2.4	2.86	13.67
MWCNT	COOH	Fe ²⁺	VitC	NO	0.3361	90	5	2.37	20
SWCNT	COOH	Fe ²⁺	NO	NO	0.3741	94.14	2.4	2.73	1
SWCNT	COOH	Fe ²⁺	VitC	NO	0.3361	90	5	2.73	1
MWCNT	COOH	Fe ²⁺	VitC	NO	0.3479	90	5	3.86	1
SW/DWCNT	OH	H ₂ O ₂	NO	NO	0.3751	300	3	3.96	1
MWCNT	OH	H ₂ O ₂	NO	NO	0.3751	300	3	2.97	13.67
MWCNT	COOH	H ₂ O ₂	NO	NO	0.3751	300	3	2.86	13.67
SWCNT	COOH	H ₂ O ₂	NO	NO	0.3751	300	3	2.73	1
MWCNT	OH	Ca ²⁺	NO	NO	0.3528	300	2.38	2.46	15.5
NO	NO	Fe ²⁺	NO	NO	0.3741	247.5	0	0	0
MWCNT	NO	Fe ²⁺	VitC	NO	0.3361	90	5	0	8
SW/DWCNT	OH	Fe ²⁺	NO	NO	0.3741	94.14	2.4	3.96	1

SW/DWCN T	OH	Fe ²⁺	VitC	NO	0.3361	90	5	3.96	1
MWCNT	OH	Fe ²⁺	NO	NO	0.3741	94.14	2.4	2.97	13.67
MWCNT	COOH	Fe ²⁺	VitC	NO	0.3361	90	5	2.86	13.67

^a $\langle V_1 \rangle = \langle t_{ij} \rangle$ (seg), $\langle V_2 \rangle = \langle c_{ij} \rangle$ ($\mu\text{g/ml}$), $\langle V_3 \rangle = \langle \text{max} W_{ij} \rangle$, $\langle V_4 \rangle = \langle \text{min} D_{ij} \rangle$ (nm)

Table 8. Simulation of $P(\%)_{\text{pred}}$ if $^{\text{max}}W_i$ and $^{\text{min}}D_i$ increase in $x(\%)$ at $t(s) = 600$ and $c(\mu\text{g/mL}) = 2.5$

CNT and Assay ^a		CNT structural parameters				$x(\%)$ increase of $^{\text{max}}W_i$ and $^{\text{min}}D_i$ ^b			
Assay	CNT	$^{\text{max}}W_i$	$^{\text{min}}D_i$	Type	Function	0	1	5	10
						$P_0(\%)$	$P_1(\%)$	$P_5(\%)$	$P_{10}(\%)$
Ca^{2+}	1	0	8	MWCNT	H	9.77	10.45	13.14	16.53
	2	3.96	1	SW/DWCNT	OH	7.89	8.51	11.03	14.18
	3	3.86	1	MWCNT	OH	7.82	8.45	10.96	14.12
	4	4	10	MWCNT	OH	13.52	14.21	16.97	20.44
	5	1.06	30	MWCNT	OH	24.28	25.11	28.43	32.60
	6	0.73	30	MWCNT	COOH	24.07	24.90	28.21	32.39
	7	4	10	MWCNT	COOH	13.52	14.21	16.97	20.44
	8	2.73	1	SWCNT	COOH	7.12	7.75	10.26	13.41
	9	3.86	1	MWCNT	COOH	7.82	8.45	10.96	14.12
Fe^{2+}	1	1	8.08	MWCNT	H	37.66	38.63	42.54	47.44
	2	4.96	1.01	SW/DWCNT	OH	34.92	35.83	39.47	44.04
	3	4.86	1.01	MWCNT	OH	34.83	35.74	39.38	43.95
	4	5	10.1	MWCNT	OH	43.08	44.08	48.08	53.10
	5	2.06	30.3	MWCNT	OH	58.67	59.87	64.68	70.72
	6	1.73	30.3	MWCNT	COOH	58.37	59.56	64.37	70.42
	7	5	10.1	MWCNT	COOH	43.08	44.08	48.08	53.10
	8	3.73	1.01	SWCNT	COOH	33.82	34.72	38.36	42.93
	9	4.86	1.01	MWCNT	COOH	34.83	35.74	39.38	43.95
H_2O_2	1	5	8.4	MWCNT	H	0	0.97	5.72	11.68
	2	8.96	1.05	SW/DWCNT	OH	0	0	1.99	7.55
	3	8.86	1.05	MWCNT	OH	0	0	1.88	7.44
	4	9	10.5	MWCNT	OH	6.38	7.59	12.46	18.57
	5	6.06	31.5	MWCNT	OH	25.34	26.80	32.65	40.01
	6	5.73	31.5	MWCNT	COOH	24.97	26.43	32.28	39.63
	7	9	10.5	MWCNT	COOH	6.38	7.59	12.46	18.57
	8	7.73	1.05	SWCNT	COOH	0	0	0.64	6.19
	9	8.86	1.05	MWCNT	COOH	0	0	1.88	7.44

^a MWCNT = Multiple-Walled, SWCNT = Single-Walled, SW/WTCNT = MWCNT + SWCNT mixture. ^b $P(\%)_{\text{pred}} = 100 \cdot [\varepsilon_{ij}(\text{CNT}+\text{TC}+\text{S})_{\text{pred}} - \varepsilon_{ij}(\text{TC}+\text{S})_{\text{obs}}] / [\varepsilon_{ij}(\text{IC}+\text{TC}+\text{S})_{\text{obs}} - \varepsilon_{ij}(\text{TC}+\text{S})_{\text{obs}}]$ is Mitoprotective protective activity, CNT = Carbon nanotube, TC = Toxic control, IC = Inhibitor control, S = Solvent. Assay details are the following. For toxicity assay 1 (a = 1), TC = Ca^{2+} , IC = CsA, and Solvent = DMSO. For assay 2 (a = 2) TC = Fe^{2+} , IC = EGTA and S = DMSO. For toxicity assay 3 (a = 3), TC = H_2O_2 , IC = Q, and Solvent = DMSO. N is the number of replicas of this assay.